Left-Right Ambiguity Resolution of a Towed Array Sonar

Katerina Kaouri
Somerville College
University of Oxford

A thesis submitted for the degree of
MSc in Mathematical Modelling and Scientific Computing

Trinity 2000

Abstract

In this work, a method is proposed for resolving the Left-Right Ambiguity in Passive Sonar Systems with towed arrays. This problem arises in source localization when the array is straight. In practice, the array is *not* straight and a statistical analysis within the Neyman-Pearson framework is developed for a monochromatic signal in the presence of random noise, assuming that the exact array shape is known. For any given array shape, an expression for the Probability of Correct Resolution (PCR) is derived as a function of two parameters; the signal to noise ratio (SNR) and an array-lateral-displacement parameter. SNR measures the strength of the signal relative to the noise and the second parameter the curvature of the array relative to the acoustic wavelength. The PCR is calculated numerically for a variety of array shapes of practical importance. The model results are found to agree with intuition; the PCR is 0.5 when the array is straight and is increasing as the signal is becoming louder and the array more curved. It is explained why the method is useful in practice and the effects of correlation between beams are discussed.

Furthermore, we look at the acoustical Sharpness Methods; these methods have originated from optical imaging, where they were used successfully to correct atmospherically degraded optical images of telescopes. The method entails that an appropriate function, called *Sharpness Function* is supposed to be maximised when the shape of the towed array, used to construct the beamformer image, is the *true* one. Reviewing carefully previous literature, which indicated that the method has good chances of producing a very good estimate of the array shape, we prove that the proposed Sharpness Function is in fact *not* maximised and we deduce that the Sharpness Method does not seem appropriate in the sonar context. Therefore, we conclude that, with the proposed Sharpness function, the Sharpness Method does not work, unlike what has been suggested in the literature. We prove however that, most crucially, Optical Imaging is the same as Beamforming. This opens avenues for further exploration of the sharpness analogy between optics and acoustics imaging.

Contents

1 Introduction **1**

1.1 The science of sonar . . . 1

1.2 Active and Passive Sonar Set . . . 1

1.2.1 Active Sonar . . . 1

1.2.2 Passive Sonar . . . 2

1.2.3 Towed Array Sonars . . . 2

1.2.4 Beamforming . . . 3

1.2.4.1 Random Noise in Beamforming . . . 5

1.2.4.2 The Directivity Function . . . 5

1.2.4.3 The Beam Pattern . . . 5

1.3 The Left-Right Ambiguity . . . 7

1.3.1 Two-Dimensional Ambiguity . . . 7

1.3.2 Three-Dimensional Ambiguity . . . 8

1.4 Possible Ways of Ambiguity Resolution . . . 8

1.5 The Sharpness Function . . . 9

2 Statistical analysis-Uncorrelated noise **11**

2.1 Statistical Testing . . . 11

2.2 Statistical Testing within Neyman Pearson Framework . . . 11

2.2.1 Statistical test for the L-R Ambiguity . . . 12

2.3 Beamforming . . . 12

2.3.1 Null Hypothesis . . . 13

2.3.2 Alternative Hypothesis . . . 14

2.4 Fourier Transforming the Beams . . . 15

2.4.1 Discrete Fourier Transform . . . 15

2.4.2 Square Law Detector . . . 16

2.4.3 DFT of Random Noise Data . . . 16

2.4.4 The Multivariate Complex Gaussian Distribution . . . 17

2.4.5 The Effect of the DFT on the SNR . . . 18
2.5 Final Formulation of the Likelihood Ratio Test . . . 19
2.5.1 Moment Generating Function of a *Non-Central* χ^2 RV . . . 20
2.5.2 Probability Density Function of a *Non-Central* χ^2 RV . . . 22
2.5.3 The Likelihood Ratio Test . . . 24
2.5.4 The Probability of Correct Resolution . . . 26

3 Applications and Numerical Simulations **27**
3.1 First Case: Sinusoid . . . 27
3.1.1 Validity of the assumption . . . 28
3.2 Second Case: Arc-of-a-Circle shape . . . 28
3.3 Numerical Results . . . 30
3.3.0.1 The Frequency for Best Ambiguity Resolution . . . 32
3.3.1 Validity of the Results . . . 32
3.3.2 One-Dimensional Plots . . . 33
3.3.2.1 Probability of Correct Resolution as $|c_0|^2$ increases (θ_s decreases), SNR *fixed* . . . 33
3.3.2.2 The Probability of Correct Resolution for SNR increasing, $|c_0|^2$ *fixed* 34

4 Statistical Analysis- Correlated Noise **36**
4.1 Correlation in the Gaussian Noise . . . 36
4.1.1 Three-Dimensional Noise Field Correlations . . . 36
4.1.2 Correlation of Two Beams . . . 37
4.1.2.1 The Discrete Fourier Transform . . . 38
4.1.3 The complex correlation coefficient . . . 39
4.1.3.1 Plots of $|\beta|$ as function of α and θ_s . . . 40
4.2 Likelihood Ratio Test in the Correlated Noise Case . . . 41
4.2.1 Hypotheses . . . 41
4.2.2 The pdf of the correlated complex random vector $\mathbf{Z}$ . . . 42
4.2.3 The joint pdf of the correlated RVs $|z_1|^2$, $|z_2|^2$ . . . 42
4.3 The Generalised Likelihood Ratio Test . . . 44
4.3.1 Hypotheses . . . 44
4.3.2 The Decision Criterion . . . 46
4.4 Conclusions . . . 46
4.5 The moment Generating Function . . . 46

5 Sharpness Function **47**

5.1 The array shape estimation problem and its effect on the beam pattern 47

5.2 Outline of Previous and Our Work 48

5.3 Beamforming formulated differently-revisiting 48

5.4 Sharpness in Optical Imaging 49

5.5 Bucker's Work 50

5.5.1 Definition of the Sharpness Function 50

5.5.2 The assumed array shape 50

5.5.3 Validity of the Worm-in-a-hole motion assumption 51

5.5.4 How the coordinates are found as the array is being towed 51

5.5.5 The Bucker Algorithm 52

5.6 Ferguson's Work ([7, 8, 9]) 53

5.7 Goris Work [12] 54

5.7.1 Analytical Work on the Sharpness Function 55

5.8 Beam Pattern is the **same** as the optical imaging 55

5.9 The proposition of new sharpness functions 58

5.10 Comparison of Acoustics and Optics 58

5.11 Drawbacks and Advantages of the Sharpness Method 59

5.12 Critical approach in Connection to the
Resolution of the Left-Right Ambiguity 60

6 Conclusions **61**

A The joint mgf of the *correlated* RVs $|z_1|^2$ and $|z_2|^2$ **63**

Bibliography **65**

List of Figures

1.1 Geometry of the Towed Array. 3
1.2 Schematic representation of the Beamforming process. 4
1.3 A beam looking at the direction $\theta = \pi/2$. 6
1.4 Two-Dimensional Ambiguity. 7
1.5 Ambiguity shown in the Beam Pattern (Straight Array). 8
1.6 Three-Dimensional Ambiguity. 8

2.1 Probability density functions if Contact is on the Right (H_0). 23
2.2 Probability density functions if Contact is on the Left (H_1). 24

3.1 Sinusoidal array shape with Number of Hydrophones = 25, $d = \lambda/2$. 28
3.2 Null Hypothesis: Contact on the Right. 29
3.3 Alternative Hypothesis: Contact on the Left. 29
3.4 The geometry for an array modelled as the arc of a circle. 30
3.5 The Probability of Correct Resolution as a function of $|c|^2 = |c_0(\alpha)|^2$ and SNR for the Sine Shape. 31
3.6 The Probability of Correct Resolution as a function of $|c_0(\theta_s)|^2$ and SNR when the array shape is the arc of a circle-θ_s ranges from 0 to $\pi/2$. 31
3.7 $|c_0|^2$ as a function of the lateral displacement parameter α. 33
3.8 $|c_0|^2$ as a function of the angle θ_s. 33
3.9 Probability of Correct Resolution as $|c_0|^2$ varies from 0 to 1 and fixed SNR= 1. . . . 34
3.10 Probability of Correct Resolution as $|c_0|^2$ varies from 0 to 1 and fixed SNR= 5. . . . 34
3.11 Probability of Correct Resolution as $|c_0|^2$ varies from 0 to 1 and SNR= 7. 35
3.12 Probability of Resolution for $|c_0|^2 = 0.0018$ and SNR varying from 1 to 10 when the array shape is sinusoidal. 35
3.13 Probability of Correct Resolution for $|c_0(\theta_s = 45^0)|^2 = 0.0429$ and SNR varying from 1 to 10-array shape is an arc with subtended angle $2\theta_s = \pi/2$. 35

4.1 $|\beta|$ as a function of α, α from 0 to 1. 41
4.2 $|\beta|$ as a function of α, α from 0 to 1.5. 41

4.3 $|\beta|$ as a function of θ_s, θ_s from 0 to $\pi/2$ 41

5.1 Muller and Buffington compensating mechanism for the implementation of the sharpness maximisation in an optical telescope, aperture plane, image plane. 50
5.2 Bucker's Algorithm. 52
5.3 The Beam Pattern before Bucker's algorithm has been implemented. 53
5.4 The Beam Pattern after Bucker's Sharpness Optimisation Algorithm. 53
5.5 The beam pattern is unreliable before the Sharpness maximisation 54
5.6 The Beam Pattern for a Conventional and an Adaptive Beamformer after Sharpness Maximisation 54

Chapter 1

Introduction

1.1 The science of sonar

The propagation of sound in the sea is a remarkably complex phenomenon. The speed of sound in seawater depends on temperature, depth, position, season of the year and salinity[1] and these factors combine in the sea to give a time-varying sound structure that is inhomogeneous both vertically and horizontally. In addition, the *attenuation* of sound in the sea has a strong frequency dependence.

In spite of these complications, sound is still the main means of exploration and communication in the sea, and the detection and processing of sound signals plays a very important role in the use of the sea both for military purposes and in other applications such as depth sounders, fish detection and divers' equipment. The science dealing with the underwater sound is called **sonar** which is an acronym for **so**und **na**vigation and **r**anging. The use of sonar was greatly advanced for military purposes during the two world wars.

1.2 Active and Passive Sonar Set

We start with some terminology. Sound can be used for underwater navigation and ranging in two main ways, which are called *active* and *passive* sonar [22].

1.2.1 Active Sonar

In active sonar, a transmitter emits sound signals which travel in the sea and reach other objects (often called *contacts* or *targets*). At these other objects the sound is scattered and some of the scatered sound returns and forms a detectable and measurable echo. The received signal is processed in order to determine the range (distance) and direction of the objects detected. This procedure followed by the active sonar (which involves a two-way transmission) is termed echo-ranging and can be very sophisticated, with directional sources and multiple receivers.

[1] the level of salt concentration in the seawater.

1.2.2 Passive Sonar

A passive sonar set ([19], [22]) has no transmitter: instead of emitting sound and receiving echoes, a passive sonar set simply *listens* for sounds made by contacts. This approach is feasible in many military contexts, because the contacts of interest (submarines, surface ships, torpedoes etc.) all make a noise. It also has the advantage (compared with active sonar) that since no sound is emitted, the sonar set does not betray its presence or position. In this work we shall deal entirely with passive sonar. Submarines are equipped with a variety of passive sonar sets, but two considerations, that are always important, are these:

(a) In order to determine the *direction* the sound is coming from, a passive sonar set must have an *array* of hydrophones (i.e. underwater microphones) to receive the sound. In order for direction to be accurately determined, the aperture (size L) of this array must be large compared with the wavelength λ of the sound involved: in fact the direction accuracy is typically of order λ/L.

(b) In order to detect a contact while it is still far off (in the far-field), it is advantageous to detect the *low* frequency sound from the contact, because this is less attenuated by seawater. (Details of the attenuation of sound in the sea, including its frequency dependence, are given in [18].)

The combined effect of these (L/λ large and λ large) is that large aperture arrays have advantages. Some passive sonar arrays are mounted on the submarine hull, but one way to get a larger aperture is to tow a long array of hydrophones behind the submarine. It is these towed array sonars that will be our concern here.

1.2.3 Towed Array Sonars

A towed array is a long flexible hose (length about $500 - 1000$m) attached to the submarine (length about $50 - 100$m) with a connecting cable (length ~ 400m). A schematic of the geometry is found in Figure 1.1.

The hose holds a large number of hydrophones which detect the incoming pressure signal and convert it to an electric signal. The signals are relayed back to the submarine and processed by the *beamformer* (see section 1.2.4) and the *beam pattern* is formed (see section 1.2.4.3).

Acoustic data from the array will often be used over several octaves in frequency. If an array of length $L = 750$m is used, then at frequency of 100Hz we have $\lambda = 15$m so $\lambda/L = 1/50$. Despite the fact that sound at 50Hz may be heard from greater ranges, it is harder to locate it, because λ/L is only $1/25$. Hence good directionality of the array is achieved if the array is at least as long as 50λ.

In addition to its large aperture, a towed array has two other advantages arising from the fact that it is not physically on the submarine:

1. The propagation of sound in the sea is best in the main sound channel, i.e the depth where the sound speed is a minimum. The array can be towed in the sound channel with the submarine

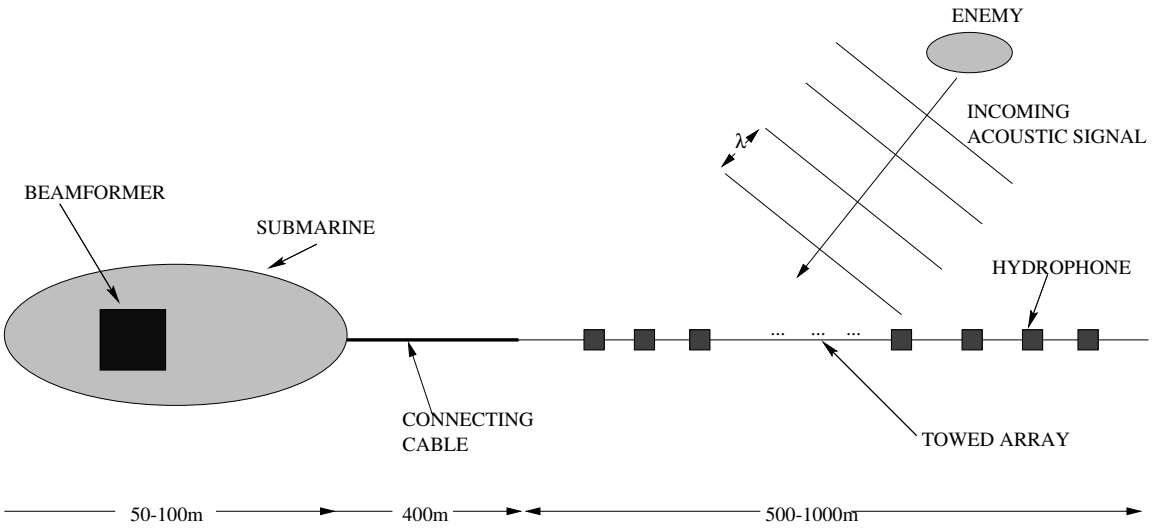

Figure 1.1: Geometry of the Towed Array.

itself not in such a large depth. In this way, the submarine can avoid detection from unfriendly vessels.

2. A submarine generates its own sound signal. Placing the hydrophones on the array, away from the submarine, reduces the level of self-noise detected by the array.

1.2.4 Beamforming

Beamforming is the process of converting the sound signals measured at different *points* into the sound signals travelling in different *directions*. The device performing this process is called *a* beamformer.

If the hydrophone positions are $\mathbf{x}_j$, $(1 \leq j \leq N_h)$, then the input to the beamformer is the set of acoustic pressure signals $p_j(t) = p(\mathbf{x}_j, t)$. If we wish to obtain from these a measure of the sound coming from the direction of a unit vector $\mathbf{u}$, then the natural approach is to form a signal

$$\boxed{b(t) = \sum_j p_j(t - \Delta_j) = \sum_j p(\mathbf{x}_j, t - \Delta_j)} \tag{1.1}$$

for time delays Δ_j chosen so that, if $p(\mathbf{x}, t)$ is a plane wave incident from direction $\mathbf{u}$, then all contributions to $b(t)$ are in phase.

For a plane wave $p = p_0 \cos(\omega t - \mathbf{k}.\mathbf{x})$ incident from direction $\mathbf{u}$, the wavevector is $\mathbf{k} = -\omega\mathbf{u}/c$, where c is the sound speed and ω is the radian frequency. Thus,

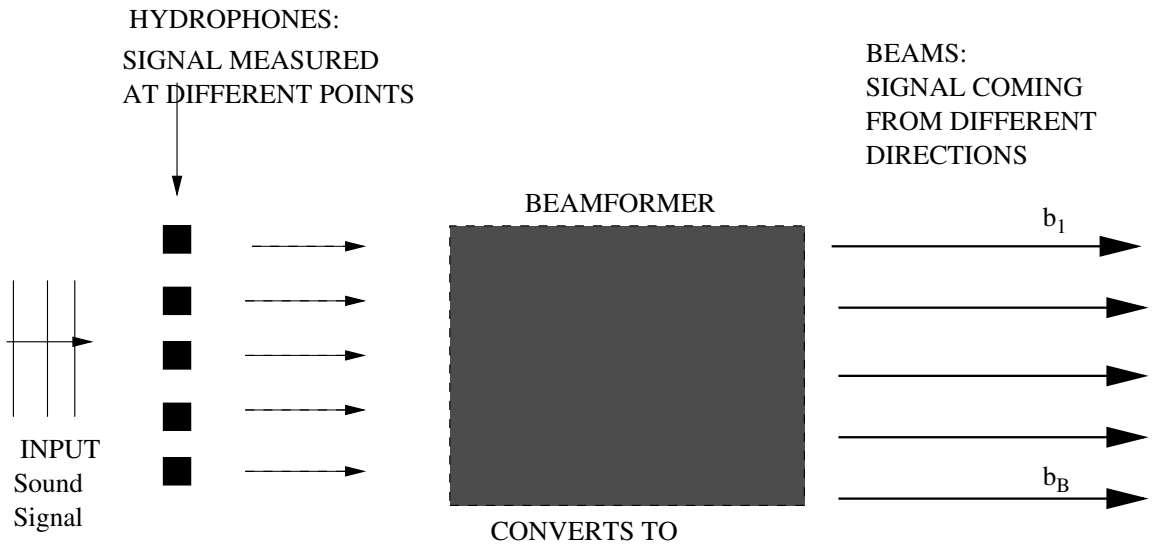

Figure 1.2: Schematic representation of the Beamforming process.

$$p_j(t-\Delta_j) = p(\mathbf{x}_j, t-\Delta_j) = p_0\cos(\omega(t-\Delta_j) - \mathbf{k}.\mathbf{x}_j) \tag{1.2}$$

$$= p_0\cos(\omega t - \omega\Delta_j + \omega\mathbf{u}.\mathbf{x}_j/c) \tag{1.3}$$

and to make all these in phase,

$$\Delta_j = \mathbf{u}.\mathbf{x}_j/c. \tag{1.4}$$

This $b(t)$ is then called the beam *looking* or *pointing* in direction $\mathbf{u}$ and the choice of Δ_j is said to *steer* the beam $b(t)$ in that direction. In practice, some offset Δ_0 may have to be applied to make all the $\Delta_j \geq 0$, and also a *weighted* sum is used so

$$b(t) = \sum_j w_j p_j(t - (\Delta_j + \Delta_0)), \tag{1.5}$$

where the w_j are called *shading* weights (and play a role analogous to a windowing function in the Fourier transform.)

The hydrophone signals can be used to form a beam pointing in *any* direction $\mathbf{u}$. In practice a set of say B beams is formed, $b_l(t)$ pointing in direction $\mathbf{u}_l$ for $1 \leq l \leq B$. Often B is chosen roughly equal to N_h.

The beam $b(t)$ has been *designed* to have maximum response to plane waves incident from direction $\mathbf{u}$.

1.2.4.1 Random Noise in Beamforming

In practice, at the jth hydrophone, along with the pressure signal p_j, sea-noise n_j is detected. Therefore the beam expression (1.1) has to be modified to include the random noise as follows:

$$b(t) = \sum_{j=1}^{N_h} w_j p(\mathbf{x}_j, t - \Delta_j) + \sum_{j=1}^{N_h} w_j n(\mathbf{x}_j, t - \Delta_j). \tag{1.6}$$

The noise sample will be modelled as a stationary Gaussian Process with zero mean (see [5], [19]). In Chapter 2, we consider this process uncorrelated in space and time while, in Chapter 4 the noise is modelled as a correlated Gaussian random process. The parameter that will measure the strength of the signal in comparison to the noise is the Signal to Noise Ratio (SNR).

The random feature of the input to the receiver due to the noise, plays an important role in this work. The presence of random fluctuations along with the deterministic signals makes the detection of these signals uncertain and the only way to look at the problem is through a statistical analysis.

1.2.4.2 The Directivity Function

To analyse the performance of the system we also need to know first how $b(t)$ responds to plane waves incident from *other* directions, and secondly how it responds to *random noise*.

First consider the response to a plane wave incident from direction $\mathbf{u}_1$, so its wavenumber is $\mathbf{k}_1 = -\omega \mathbf{u}_1/c$. Then

$$\begin{aligned} b(t) &= \sum_j w_j p(\mathbf{x}_j, t - \Delta_j) \\ &= \sum_j w_j p_0 \cos(\omega(t - \Delta_j) + \omega \mathbf{u}_1.\mathbf{x}_j/c) \\ &= \Re(p_0 e^{i\omega t} G_b(\mathbf{u}_1, \omega)), \end{aligned} \tag{1.7}$$

where

$$\begin{aligned} G_b(\mathbf{u}_1, \omega)) &= \sum_j w_j \exp(i\omega \mathbf{u}_1.\mathbf{x}_j/c - i\omega\Delta_j) \\ &= \sum w_j \exp(i\omega(\mathbf{u}_1 - \mathbf{u}).\mathbf{x}_j/c), \end{aligned} \tag{1.8}$$

if Δ_j are given by $\mathbf{u}.\mathbf{x}_j/c$. G_b will be called the directivity function of beam b: it expresses how the beam responds to sound incident from any direction $\mathbf{u}_1$ and is maximised when the beam 'looks' in the direction of arrival. We shall show later (Chapter 4) that the response of $b(t)$ to random noise can also be represented in terms of G_b.

1.2.4.3 The Beam Pattern

In practice, the Beam Pattern is created by plotting $D(\theta) = 20\log_{10}(|G(\theta)|/\max_\theta |G(\theta)|)$ against the θ range $[0, 2\pi]$ (which represents all the possible signal incidence directions). In Figure 1.3 we

plot $D(\theta)$ for the beam looking in direction $\theta_b = \pi/2$. As we have already said, by construction $D(\theta)$ is maximised at $\theta = \theta_b$ and forms a so-called *mainlobe* as it can be seen in 1.3. All the beams looking in directions other than $\pi/2$ give rise to sidelobes in the beampattern.

The *beam centre* b_c is defined to be the average value of θ over those directions in which $D(\theta)$ is within 6dB of its maximum. Ideally the beam centre should be at the steering angle θ_b. The *beam width* b_w is defined as the width of the main lobe when $D(\theta)$ is 3dB below the peak of the lobe. In Figure 1.3 we pointed b_w and b_c for the beam looking at direction $\theta = \pi/2$.

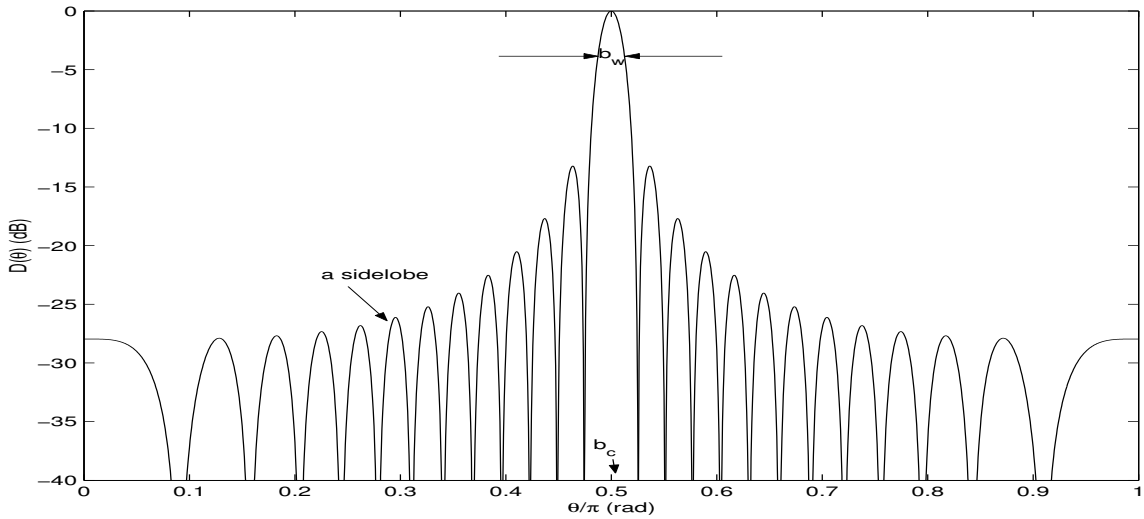

Figure 1.3: A beam looking at the direction $\theta = \pi/2$.

1.3 The Left-Right Ambiguity

We are now ready to describe the ambiguity problem we are addressing in this work.

1.3.1 Two-Dimensional Ambiguity

Description

A major difficulty faced by a submarine trying to detect a threat is to resolve whether the contact vessel detected by a towed array is on the *left* or the *right* of the submarine.

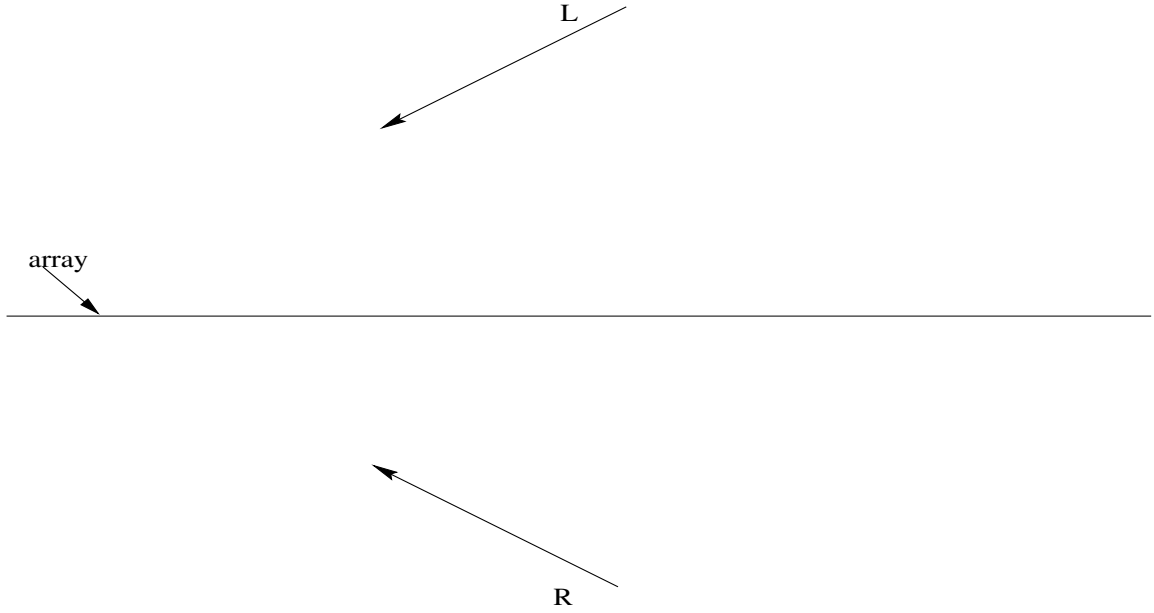

Figure 1.4: Two-Dimensional Ambiguity.

The incoming plane waves in Figure 1.4 above, denoted L/R for Left/Right respectively, are indistinguishable if the array is straight. This ambiguity exhibits itself on the beam pattern with the presence of one mainlobe at the angle θ and a identical, perfectly-correlated sidelobe at the angle $-\theta$, where θ is the incident angle of the wave. This ambiguity can been in the beam pattern in Figure 1.5 (where $\theta = \pi/2$).

Until now, this obviously troublesome ambiguity has not been resolved theoretically and in this work, under certain assumptions, we achieve to carry this task through.

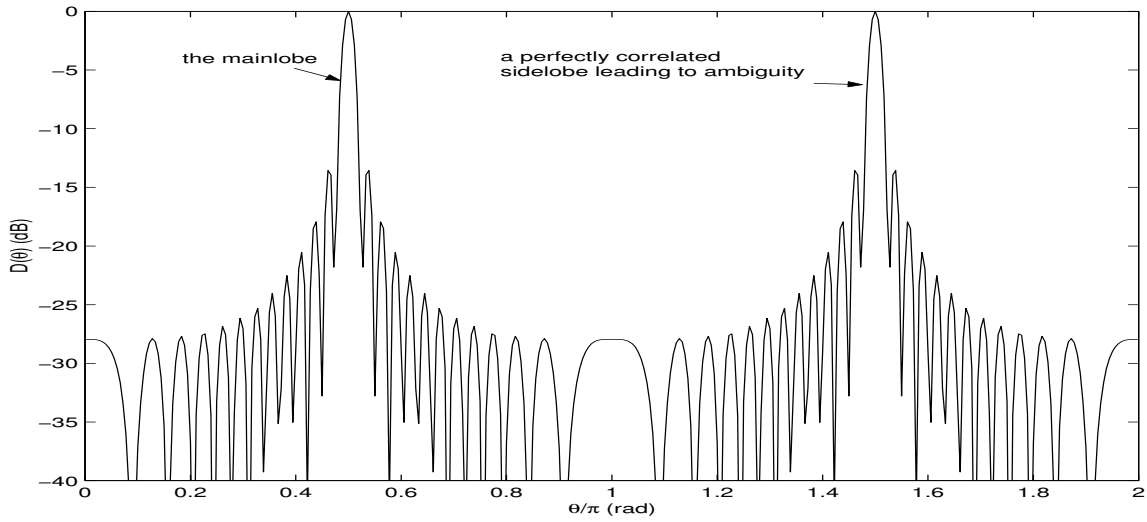

Figure 1.5: Ambiguity shown in the Beam Pattern (Straight Array).

1.3.2 Three-Dimensional Ambiguity

The three-dimensional analogue of the above problem is that the incoming plane wave along any generator of the cone in Figure 1.6 below is indistinguishable by a submarine with a straight array shape.

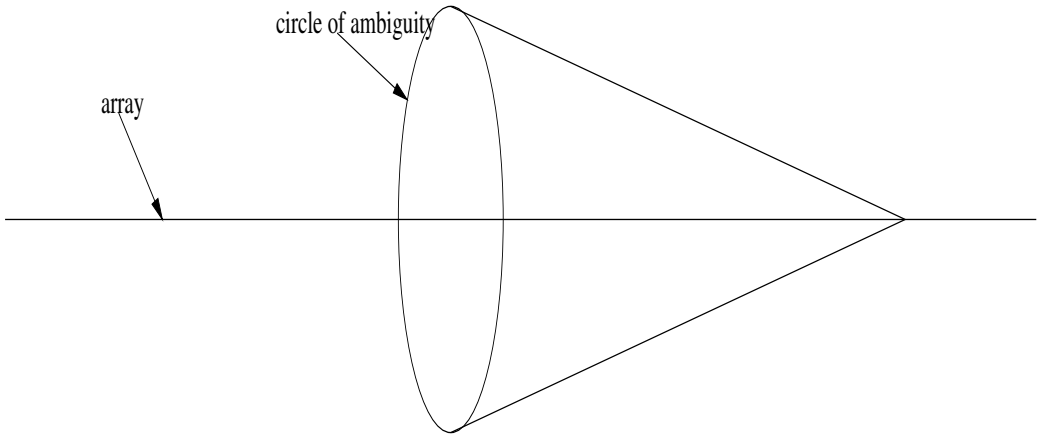

Figure 1.6: Three-Dimensional Ambiguity.

1.4 Possible Ways of Ambiguity Resolution

Various methods have been proposed in order to resolve this troublesome ambiguity of which we mention the most significant ones below.

(a). One proposed way of resolving this ambiguity constitutes of the submarine turning, say, 10^0

to the left or right while watching whether θ_{contact} increases or decreases. This method is however undesirable, because such a manoeuvre may bring the submarine towards the contact vessel, which make its detection by a threat contact much easier.
(b). Another way is to tow twin arrays instead of a single array, which increases the directionality of the array, disrupting the undesirable symmetry in the beam pattern which results from the array being straight. Although this method is used by ships, it is quite unsuitable for a submarine where extremely tight space constraints have to be met, and where the two arrays would have to be deployed and recovered very fast.
(c). The third way exploits the fact that, in the sea, the array is never exactly straight. Assuming a non-straight array breaks the undesirable symmetry of the beam pattern that was observed in Figure 1.4.

We are going to use the third way to construct formal mathematical means for measuring the ambiguity. Whether the resolution of the ambiguity has been achieved will be judged by calculating the *probability of correct resolution*.

Determining an accurate enough array shape is a formidable task of its own since it is affected by ocean waves, swell of the array, route corrections, drag and other factors. We discuss more on this matter on the following section and in Chapter 5.

In this dissertation we are exploring this third method of ambiguity resolution. We take as test cases: a). the array shape is one-cycle of a sine wave, b). the array shape is the arc of a circle. The first case is applicable when the submarine is steering in a zig-zag manner as may happen often and the second case is appropriate for analysing a submarine turn (change in course).

In Chapter 2 we define the ambiguity problem in precise terms. Under the assumption of an uncorrelated noise field we use the inherent statistical information to calculate the probability of resolution as a function of the curvature of the array and the Signal to Noise Ratio.

In Chapter 4 we consider a three-dimensional correlated noise field and we aim to quantify again the probability of correct resolution. We also aim to study the behaviour of the correlation coefficient characterising the *correlated* noise field.

1.5 The Sharpness Function

The certainty with which we can decide whether a contact is on the left or the right depends to a large extent on the precision with which the beam pattern is constructed. An accurate pattern will obviously increase the probability of ambiguity resolution.

The precision of the beam pattern is directly related with the shape of the array; it is clear that to achieve an accurate beam pattern we need to know with accuracy the shape of the array at each instant. If there is a large error in the calculation of the array shape, even if the array is long enough

for good directionality, the beamformer forms wide beams with the consequence that the contact cannot be localised to a particular direction.

It is almost impossible however to determine the exact shape of the array[2] and although many methods have been proposed, the problem of accurate array shape estimation can still be considered open.

In this work we also aim to discuss means of sharpening the beam pattern. The key notion for this is the *sharpness function*. A Sharpness Function is defined as a/the function that it is maximised when the beamformer is using the *correct* array shape.

Such a sharpness function has been proposed by H.P.Bucker[4] in 1978 in connection with an analogous function in the Optics literature ([13], [15]), used to sharpen in real-time images of stars at telescopes. This optical function is maximised when the resolution of the star image, that underwent distortions due to atmospheric turbulence, becomes the best possible (diffraction-limited).

However, the Bucker proposition has not been implemented by any submarine mechanism until now as simulations performed with this method proved inconclusive for the validity of the method.

We have investigated the Bucker Sharpness Function analytically and found that it is not maximised when the assumed array shape becomes the true array shape. However, we show at the same time that noise-free beamforming and optical imaging are completely analogous.

Furthermore, we propose two modified sharpness functions which take into account more characteristics of the underlying geometry.

We finally draw the similarities and differences between Optics and Acoustics and we give a conclusion about the validity of the Sharpness Method. The aforementioned investigations are carried out in Chapter 5.

[2]This shape is affected by ocean waves, swell of the array, course corrections, hydrodynamics, drag etc.

Chapter 2

Statistical analysis-Uncorrelated noise

2.1 Statistical Testing

We are aiming to develop a statistical analysis framework with which we can determine with some quantifiable confidence whether the contact is on the left or the right and thus resolve the left-right ambiguity. The tool that will help us treat the ambiguity is the use of the fact that the array is not straight[1].
We expect that a good resolution will be achieved if the Signal to Noise Ratio and the lateral displacement of the array in comparison with the incident wavelength are sufficiently large.

2.2 Statistical Testing within Neyman Pearson Framework

Statistical hypothesis testing is a formal means of distinguishing between probability distributions on the basis of random variables generated from one of the distributions. In the Neyman-Pearson framework the **probability distributions** or **probability density functions**(p.d.fs) are classed into two possibilities; the first one is called the **null hypothesis** and is denoted by H_0 and the other the **alternative hypothesis** and is denoted by H_1.

According to the Neyman-Pearson approach, a decision as to whether or not to reject the null hypothesis H_0 in favour of H_1 is made by looking at the value of $T(\mathbf{x})$ where $\mathbf{x}$ denotes the sampled data and $T(\mathbf{x})$ is called the **statistic**. The set of values of T for which H_0 is accepted is called the **acceptance region** and the values of T for which the H_0 is rejected is called the **rejection** or

[1] as we mentioned in the Introduction there are also other ways with which the Ambiguity Resolution could be handled but we consider this method the most appropriate for a submarine.

critical region. We also define the quantities

$$\begin{aligned}\mathbf{P}(H_0 \text{ rejected } |H_0 \text{ true }) &= \textbf{Type I error} = \alpha \\ \mathbf{P}(H_0 \text{ accepted } |H_0 \text{ false }) &= \textbf{Type II error} = \beta\end{aligned} \tag{2.1}$$

and

$$\mathbf{P}(H_0 \text{ rejected } |H_0 \text{ false }) = 1-\beta = \textbf{Power} \text{ of the test}$$

Often the critical region is of the form $\{T > t_C\}$. In such a case, the number t_C is called the **critical value** of the test; the critical value separates the critical and the acceptance region.

There are typically many tests with significance level α possible for a null hypothesis versus an alternative hypothesis. From those we would like to select the *optimum* test, in the sense that for any given α the power of the test $(1-\beta)$ is *maximised*.

A test satisfying this property is called the **Likelihood Ratio Test** (LRT) as stated by the Neyman-Pearson lemma (see [10], [17]). Suppose that under the hypothesis H_0 the probability density function is $f_0(\mathbf{x})$ and that the pdf under hypothesis H_1 is $f_1(\mathbf{x})$. Given observed data $\mathbf{x}$, the relative plausibilities of H_0 and H_1 are measured by the likelihood ratio $L = f_1(\mathbf{x})/f_0(\mathbf{x})$. If the ratio is large then the data is more likely under the alternative hypothesis H_1 and the Likelihood Ratio Test rejects the null hypothesis for large values of the likelihood ratio. This is the type of test we employ in this work.

2.2.1 Statistical test for the L-R Ambiguity

For resolving the Left-Right Ambiguity we will choose our hypotheses as follows:

Null Hypothesis:

H_0:"Contact is on the Right".

Alternative Hypothesis:

H_1:"Contact is on the Left".

It is obvious that there is no reason to choose one of the two assumptions as being the null one. This symmetry between H_0 and H_1 will also be exhibited in the following analysis.

2.3 Beamforming

For simplicity, we imagine a Beamformer that forms only two beams: Left and Right Broadside. The analysis would be very similar for resolving the ambiguity between $\pm\theta$ for a general angle θ. Suppose we have the incident wave

$$p = p_0 e^{i(\omega t + \mathbf{k}.\mathbf{x})}, \tag{2.2}$$

where we assume the real part.

Note:

k in this chapter is in a direction opposite to the direction of propagation as it is the usual convention (also kept in the rest of the chapters). However, we will see that the statistical test and consequently the Probability of Correct Resolution depends only on the square modulus of the complex quantities and therefore nothing in the following analysis is affected by this sign change.

For an incident wave coming from the right(null hypothesis) the wavevector **k** simplifies to $\mathbf{k} = (0, k)$ and hence the pressure field is given by $p(y,t) = p_0 e^{i(\omega t + ky)}$, which is independent of x. We can therefore write down the pressure signal at the jth hydrophone:

$$p_j(t) = p_0 e^{i(\omega t + k y_j)}. \tag{2.3}$$

We now form the Right and Left beams under the assumption that the contact is on the Right, and we denote those as b_{RR} and b_{RL} respectively. The first subscript signifies if the contact is on the L or the R and the second subscript the beam direction. Hence, the Right and Left beam, under the assumption that the contact is on the left (alternative hypothesis), are denoted by b_{LR} and b_{LL} respectively.

We apply the beamforming analysis of the Introduction in the case of an incoming *plane* wave with incidence vector $\mathbf{u} = (\cos\theta, \sin\theta)$. Hence the time delays introduced by the beamformer when the steering angle is θ_b are

$$\Delta_j(\theta_b) = \frac{x_j \cos\theta_b + y_j \sin\theta_b}{c} \tag{2.4}$$

and then from (2.3)

$$p_j(t - \Delta_j(\theta_b)) = p_0 \exp(i\omega t) \exp(iky_j(1 - \sin\theta_b)) \exp(-ikx_j \cos\theta_b). \tag{2.5}$$

2.3.1 Null Hypothesis

For $\theta_b = \frac{\pi}{2}$ the time delay (2.4) simplifies to

$$\Delta_j = \frac{y_j}{c}. \tag{2.6}$$

The Right Broadside Beam $b_{RR}(t)$, using (2.3) and (2.6), is given by:

$$\begin{aligned} b_{RR}(t) &= \sum_{j=1}^{N_h} p_0 \exp\left(i\omega(t - \frac{y_j}{c} + \frac{y_j}{c})\right) + \sum_{j=1}^{N_h} n_j(t - \Delta_j) \\ &= p_0 e^{i\omega t} G(\theta = \frac{\pi}{2}, \theta_b = \frac{\pi}{2}, \omega) + \sum_{j=1}^{N_h} n_j(t - \Delta_j) \end{aligned} \tag{2.7}$$

where

$$G_{RR} = G(\theta = \frac{\pi}{2}, \theta_b = \frac{\pi}{2}, \omega) = \sum_{j=1}^{N_h} 1 = N_h \tag{2.8}$$

is the gain introduced by the array.

For the Left Broadside Beam $b_{RL}(t)$ the time delays are given by

$$\Delta_j = -\frac{y_j}{c} \tag{2.9}$$

and b_{RL} is given as follows:

$$\begin{aligned} b_{RL}(t) &= \sum_{j=1}^{N_h} p_0 \exp\left(i\omega(t + \frac{y_j}{c} + \frac{y_j}{c})\right) + \sum_{j=1}^{N_h} n_j(t - \Delta_j) \\ &= p_0 e^{i\omega t} G(\theta = \frac{\pi}{2}, \theta_b = \frac{3\pi}{2}, \omega) + \sum_{j=1}^{N_h} n_j(t - \Delta_j) \end{aligned} \tag{2.10}$$

where

$$G_{RL} = G(\theta = \frac{\pi}{2}, \theta_b = \frac{3\pi}{2}, \omega) = \sum_{j=1}^{N_h} \exp\left(\frac{2i\omega y_j}{c}\right) \tag{2.11}$$

is the gain introduced by the array. Note that $|G_{RR}| > |G_{RL}|$ since $|\exp(2i\omega y_j/c)| < 1$.

2.3.2 Alternative Hypothesis

Now the incoming wave is $\mathbf{k} = (0, -k)$. Following the same way as for the null hypothesis, we form b_{LR} and b_{LL}:

$$b_{LR}(t) = p_0 e^{i\omega t} G(\theta = \frac{3\pi}{2}, \theta_b = \frac{\pi}{2}, \omega) + \sum_{j=1}^{N_h} n_j(t - \Delta_j), \tag{2.12}$$

where now the gain introduced by the array is

$$G_{LR} = G(\theta = \frac{3\pi}{2}, \theta_b = \frac{\pi}{2}, \omega) = \sum_{j=1}^{N_h} \exp\left(-\frac{2i\omega y_j}{c}\right). \tag{2.13}$$

Note that $G_{LR} = \overline{G}_{RL}$. For the left beam the time delays are $\Delta_j = -y_j/c$ and hence

$$b_{LL}(t) = p_0 e^{i\omega t} G(\theta = \frac{3\pi}{2}, \theta_b = \frac{3\pi}{2}, \omega) + \sum_{j=1}^{N_h} n_j(t - \Delta_j) \tag{2.14}$$

and the gain is given by

$$G_{LL} = G(\theta = \frac{3\pi}{2}, \theta_b = \frac{3\pi}{2}, \omega) = \sum_{j=1}^{N_h} 1 = N_h. \tag{2.15}$$

We notice that each of the four beam possibilities can be expressed as

$$b = p_0 N_h \Re(c_0 \exp(i\omega t)) \tag{2.16}$$

where c_0 is given by

$$c_0 = \frac{1}{N_h} \begin{cases} N_h & \text{for } b_{RR}(t), \\ \sum \exp(2i\omega y_j/c) & \text{for } b_{RL}(t), \\ \sum \exp(-2i\omega y_j/c) & \text{for } b_{LR}(t), \\ N_h & \text{for } b_{LL}(t). \end{cases}$$

In practice, the beams are sampled at discrete times and the Discrete Fourier Transform (DFT) of the Beams is taken. Afterwards, the *kth* component of the DFT vector is squared using the so-called 'Square-Law Detector' where k is the frequency of interest ($\omega = 2\pi k$). We assume a narrowband signal, that is the frequency spectrum is concentrated at a *single* frequency. We give a brief survey of those operations in the following section.

2.4 Fourier Transforming the Beams

2.4.1 Discrete Fourier Transform

We assume that in a period of $T = 1s$ we sample the incoming signal (and noise) M times in equal time-intervals $\Delta t = \frac{1}{M}$ and hence the discretised time is $t_m = \frac{m}{M}$. For the real valued time-series $s_1, ..., s_M$, the Discrete Fourier transform(DFT) is:

$$\hat{S}_r = \sum_m s_m e^{-2\pi i r m/M} \tag{2.17}$$

- $\hat{S}_r$ is a complex Hermitian sequence and $\hat{S}_{-r} = \hat{S}_r^\star$ where $\star$ stands for complex conjugate.
- $\hat{S}_r$ is periodic with period M in the integer variable r, that is $\hat{S}_{r+M} = \hat{S}_r$. Often M is even and r ranges from $-M/2 + 1, ..., M/2$.

Since all beams are of the form (2.16) we look want to take the DFT of the time series $s_m = \Re(c_0 \exp(2\pi i m k/M))$. Then,

$$\hat{S}_r = \sum_m \Re(c_0 \exp(2\pi i m k/M)) e^{-2\pi i r m/M}, \tag{2.18}$$

and representing $c_0 = |c_0| \exp(i\delta)$

$$\hat{S}_r = \frac{1}{2}|c_0| \sum_m \left(e^{i\delta} \exp(2\pi i m(k-r)/M) + e^{-i\delta} \exp(-2\pi i m(k+r)/M) \right). \tag{2.19}$$

Then

$$\hat{S}_r = 0 \quad \forall r \neq k, -k \text{ and} \tag{2.20}$$

$$\hat{S}_k = |c_0| e^{i\delta} \frac{M}{2} = \hat{S}_{-k}^\star \tag{2.21}$$

where the phase information in each beam is given by[2]

[2]We use $\sum \exp(2i\omega y_j/c) = \sum \cos(2\omega y_j/c) + i \sum \sin(2\omega y_j/c)$.

$$\delta = \begin{cases} 0 & \text{for } b_{RR}(t), \\ \arctan\left(\sum \sin(2\omega y_j/c)/\sum \cos(2\omega y_j/c)\right) & \text{for } b_{RL}(t), \\ -\arctan\left(\sum \sin(2\omega y_j/c)/\sum \cos(2\omega y_j/c)\right) & \text{for } b_{LR}(t), \\ 0 & \text{for } b_{LL}(t). \end{cases}$$

2.4.2 Square Law Detector

A **square law detector** forms the values $Y_r = |\hat{S}_r|^2$ for $0 \leq r \leq M/2$. Y_k measures how much of the power of the signal is concentrated at the frequency k.

$$Y_r = 0 \quad \forall r \neq k \tag{2.22}$$

$$Y_k = |c_0|^2 \frac{M^2}{4} \tag{2.23}$$

Note that all the information about the phase of the signal is thrown away. This loss does not allow the restoration of the signal from the values Y_r, that is we *cannot* find s_m using the Inverse Fourier Transform (IFT)

$$s_m = \frac{1}{M} \sum_r \hat{S}_r e^{-2\pi r m/M}. \tag{2.24}$$

However, Parseval's formula gives

$$\sum_m |s_m|^2 = \frac{1}{M}(Y_0 + 2Y_1 + ... + 2Y_{M/2-1} + Y_{M/2}). \tag{2.25}$$

This says that the *'energy in the time-domain'='energy in the frequency domain'* and hence we can determine from Y_r the energy of the incoming signal and how it is distributed over frequency.

2.4.3 DFT of Random Noise Data

We assume that the incoming noise $n(\mathbf{x}, t)$ is an isotropic stationary, Gaussian, random process. We sample the noise at a *fixed* spatial location on the array in exactly the same way we sampled the signal so that we again have a time sample of size M drawn from the random process. We can represent this sample by the vector

$$\mathbf{n} = (n_1, ..., n_M)^T$$

- $n_m = n(\mathbf{x}, t_m)$ is a real Gaussian Random Variable with mean zero and Variance $\mathbb{E}(|n_m|^2) = \sigma^2$.
- The components of $\mathbf{n}$ are statistically independent.

These two features of $\mathbf{n}$ can be summarised by writing the covariance matrix as

$$\mathbb{E}(\mathbf{n}\mathbf{n}^\dagger) = \sigma^2\mathbf{I} \tag{2.26}$$

where $\mathbf{I}$ is the identity matrix.
We will denote the Discrete Fourier Transform of $\mathbf{n}$ by $\mathbf{N}$.

$$\begin{aligned} N_r &= DFT(n_m) \\ &= \sum_{m=1}^{M} F_{rm} n_m \end{aligned} \tag{2.27}$$

This can be written in matrix form $\mathbf{N} = F\mathbf{n}$ where

$$F_{rm} = e^{-2\pi i r \frac{m}{M}}. \tag{2.28}$$

The random variable N_r is a *complex* Gaussian random variable with zero mean since

$$\mathbb{E}(N_r) = \sum_m F_{rm}\mathbb{E}(n_m) = 0 \tag{2.29}$$

The covariance matrix of $\mathbf{N}$ is given by

$$\mathbb{E}(\mathbf{N}\mathbf{N}^\dagger) = \mathbb{E}\left(F\mathbf{n}\mathbf{n}^\dagger F^\dagger\right) \tag{2.30}$$

$$= F\mathbb{E}\left(\mathbf{n}\mathbf{n}^\dagger\right)F^\dagger \tag{2.31}$$

$$= \sigma^2 F F^\dagger \quad \text{using (2.26).} \tag{2.32}$$

Since F_{rm} is given by (2.28) we have obviously that

$$(FF^\dagger)_{rs} = M\delta_{rs}. \tag{2.33}$$

Hence (2.32) becomes

$$\mathbb{E}(\mathbf{N}\mathbf{N}^\dagger) = \sigma^2 M\mathbf{I}. \tag{2.34}$$

From (2.29) and (2.34) we deduce that the components of $\mathbf{N} = \{N_r\}$ are statistically independent, *complex Gaussian* Random Variables with zero mean and variance= $E(|N_r|^2) = M\sigma^2$.

As we have already mentioned, until this point we have not taken into account the presence of the towed array; the above DFT of data refers to a *fixed* spatial location $\mathbf{x}$.

2.4.4 The Multivariate Complex Gaussian Distribution

A p-variate Complex Gaussian RV (C.G.R.V) $\mathbf{Z}$ is a p-tuple of complex Gaussian random variables such that the vector of real and imaginary parts is $2p$-variate Gaussian distribution (we make the assumption that the means are zero). The correlations among the elements of the multivariate vector

are represented by a $2p \times 2p$ *real* covariance matrix or equivalently an *isomorphic* $p \times p$ Hermitian covariance matrix. In this work we choose the latter representation and we make use of the following pdf of the a p-variate C.G.R.V given by

$$f(\mathbf{Z}) = \frac{1}{\pi^p \det V} e^{(-\mathbf{Z}^\dagger V^{-1} \mathbf{Z})} \tag{2.35}$$

where V is the Hermitian covariance matrix.

The theory of a multivariate C.G.R.V is counterpart of the classical multivariate real Gaussian statistical analysis. However, the complex statistical Analysis can be considered richer than the real analogue because not all results of the complex case are counterparts of the real case. More details on the C.G.R.V. can be found in [11] and [20].

2.4.5 The Effect of the DFT on the SNR

We write

$$D_k = \frac{p_0 M}{2} + N_k$$

to be the kth component of the DFT of the incoming data at a fixed spatial location (no beamforming as yet) where $p_0 M/2$ is the DFT of the signal and N_k is the kth component of the DFT of the incoming noise. D_k is a complex Gaussian variable with mean $p_0 M/2$ and variance $M\sigma^2$. Consequently, $|D_k|^2$ is a non-central χ^2 with two degrees of freedom and the non-centrality parameter $(p_0 M/2)^2$. For an exposition of the statistics of a χ^2 RV see section 2.5.1. Then, by definition, the Signal to Noise Ratio in the Frequency domain is:

$$\begin{aligned} \text{SNR} &= \left(\frac{p_0 M}{2}\right)^2 / (M\sigma^2) && (2.36) \\ &= \left(\frac{M}{2}\right)\Big(\underbrace{\frac{p_0^2}{2\sigma^2}}_{\text{SNR in time domain}}\Big) && (2.37) \end{aligned}$$

We see that with the use of the Fourier Transform the SNR has been magnified by a factor of $M/2$. The DFT improves the SNR by using the fact that the signal is at a *particular* frequency. (Note that also the beamformer improves the SNR, using the fact that the signal comes from a *particular* direction.)

In the following part we are proceeding with the assumption that the incoming sea-noise is uncorrelated both spatially and temporally. Although this assumption is not generally true for small lateral displacements of the array, we consider the relevant analysis as it gives valuable insight on the statistical testing procedure. A more detailed analysis, dropping this assumption, is undertaken in Chapter 4.

2.5 Final Formulation of the Likelihood Ratio Test

For the null hypothesis, 'Contact on the Right', we will look only at the kth component of the DFT of the beams $b_{RR}(t)$ and $b_{RL}(t)$ where those are meant to include both the effect of the signal and the noise. From now on we call the frequency of interest f (for symbolic reasons) and we change the subscripts to 1 and 2 for Right and Left respectively.

Under H_0:

$$b_1 = a + N_1 \tag{2.38}$$

where $a = p_0 M N_h/2$ and N_1 is a complex Gaussian Random Variable with zero mean and variance $\mathbb{E}(|N_1|^2) = M\sigma^2 = \xi^2$. We write

$$N_1 = \Re N + i\Im N \tag{2.39}$$

According to the way the square-law detector works we form:

$$\begin{aligned} |b_1|^2 &= (a + N_1)(a + \bar{N_1}) && (2.40)\\ &= a^2 + 2a(N_1 + \bar{N_1}) + N_1\bar{N_1} = a^2 + 2a\Re N_1 + |N_1|^2 && (2.41) \end{aligned}$$

Hence we have

$$\mathbb{E}(|b_1|^2) = a^2 + \xi^2 \tag{2.42}$$

and the Signal to Noise Ratio in this beam is given by

$$(\text{SNR})_1 = \frac{a^2}{\xi^2} \tag{2.43}$$

Most frequently, in practice,the SNR is converted to decibels through $10\log_{10}(a^2/\xi^2) = 20\log_{10}(a/\xi)$. We also have

$$b_2 = c_0 a + N_2 \tag{2.44}$$

where c_0 is the *complex* parameter

$$c_0 = \frac{1}{N_h}\sum_{j=1}^{N_h} \exp(i\frac{4\pi f y_j}{c}), \tag{2.45}$$

and contains the information about the array shape.

The noise in the second beam, N_2, has identical statistical properties with N_1 (since we assumed that the noise is isotropic) and the pdf of the vector $\mathbf{N}_{12} = (N_1, N_2)^T$ is given by:

$$f(\mathbf{N}_{12}) = \frac{1}{\pi^2 \det V} e^{(-\mathbf{N}_{12}^\dagger V^{-1}\mathbf{N}_{12})} \tag{2.46}$$

Hence

$$E(|b_2|^2) = |c_0|^2|a|^2 + \xi^2. \tag{2.47}$$

The SNR in this beam is given by $(\text{SNR})_2 = |c_0|^2 a^2/\xi^2 = |c_0|^2(\text{SNR})_1$, where

$$|c_0|^2 = \frac{1}{N_h^2}\sum_j \exp(\frac{4\pi i f y_j}{c})\sum_j \exp(-\frac{4\pi i f y_j}{c}) \tag{2.48}$$

$$= \frac{1}{N_h^2}\left(\left[\sum_j \cos(\frac{4\pi f y_j}{c})\right]^2 + \left[\sum_j \sin(\frac{4\pi f y_j}{c})\right]^2\right) \tag{2.49}$$

Therefore $|c_0| < 1$ which indicates that the signal in the right beam is louder, as we indeed expect under the assumption that the contact is on the right.

Both $|b_1|^2$ and $|b_2|^2$ are characterised by probability density functions of which the means are respectively (2.42) and (2.47) above. (It will be shown that these p.d.f.s are related to the non-central χ^2 distribution and the details are given in the next section.)

Under the Alternative Hypothesis H_1:'Contact on the Left', we need to consider instead the beams $b_{LL}(t)$ and $b_{LR}(t)$. Hence b_1 and b_2 are

$$b_1 = \bar{c_0}a + N_1, \tag{2.50}$$

$$b_2 = a + N_2. \tag{2.51}$$

where c_0 and a as defined above. We then find

$$E(|b_1|^2) = |c_0|^2a^2 + \xi^2 \tag{2.52}$$

$$E(|b_2|^2) = a^2 + \xi^2 \tag{2.53}$$

as the means of the random variables under H_1.

We now set off for the derivation of quantitative expressions of the statistical properties of $|b_1|^2$ and $|b_2|^2$.

2.5.1 Moment Generating Function of a *Non-Central* χ^2 RV

We will work initially in the general framework of n complex Gaussian random variables Z_l with a *non-zero* mean. We let

$$Z_l = \mu_l + X_l \tag{2.54}$$

where μ_l is complex and deterministic and X_l is a complex Gaussian RV of which the real and imaginary part are statistically independent and distributed as *real, standard* normal RVs. We form the random variable

$$T = \sum_{l=1}^{n} |\mu_l + X_l|^2 \tag{2.55}$$

$$= \sum_{l} (\Re(\mu_l + X_l))^2 + (\Im(\mu_l + X_l))^2 \tag{2.56}$$

where $\Re$ stands for the real part and $\Im$ stands for the imaginary part.

The moment generating function of T is given by

$$\text{mgf(T)} = \mathbb{E}(e^{sT}) \tag{2.57}$$

$$= \text{mgf}(\sum_{\text{l}} (\Re(\mu_{\text{l}} + \text{X}_{\text{l}}))^2)\text{mgf}(\sum_{\text{l}} (\Im(\mu_{\text{l}} + \text{X}_{\text{l}}))^2) \tag{2.58}$$

Since the real and imaginary part of X_l are independent (because the noise field is assumed to be uncorrelated), $\sum_l (\Re(\mu_l + X_l))^2$ and $\sum_l (\Im(\mu_l + X_l))^2$ are independent We consider the mgf of either $\sum_l (\Re(\mu_l + X_l))^2$ (or $\sum_l (\Im(\mu_l + X_l))^2$) and since the relevant manipulations concerning $\Re$ and $\Im$ part are identical, in the following calculation it is sufficient to calculate using only $\Re$. Consider

$$\text{mgf(Z)} = \mathbb{E}\left(\exp(\text{s}\sum_{\text{l}} (\Re(\mu_{\text{l}} + \text{X}_{\text{l}}))^2)\right) = \prod_{l=1}^{n} \mathbb{E}\left(\exp(s(\Re(\mu_l + X_l))^2\right) \tag{2.59}$$

$$= \prod_{l=1}^{n} \left(\frac{1}{\sqrt{2\pi}} \int_{-\infty}^{\infty} \exp\left(s(\Re(\mu_l + X_l))^2\right) \exp\left(-\frac{{x_l}^2}{2}\right) dx_l\right) \tag{2.60}$$

Taking constant terms out and completing the square,

$$= \exp\left(s\sum_{l} (\Re\mu_l)^2\right) \exp\left(\frac{s^2}{(1/2 - s)} \sum_{l} (\Re\mu_l)^2\right) \times$$

$$\prod_{l=1}^{n} \left(\frac{1}{\sqrt{2\pi}} \int_{-\infty}^{\infty} \exp\left(-(\frac{1}{2} - s)\left(x_l - \frac{s\mu_l}{\frac{1}{2} - s}\right)^2\right) dx_l\right)$$

$$= \exp\left(\frac{s}{1 - 2s} \sum_{l} (\Re\mu_l)^2\right) (1 - 2s)^{-n/2} \tag{2.61}$$

which is the mgf of a non-central χ^2_n distribution with non-centrality parameter $\sum_l (\Re\mu_l)^2$. From now on we will denote this distribution by $\chi^2_n(\lambda)$ where λ is the non-centrality parameter.

• Note: $(1 - 2t)^{-n/2}$ is the mgf of a χ^2_n distribution.

Hence

$$\text{mgf(T)} = E(e^{sT}) \tag{2.62}$$

$$= \exp\left(\frac{s}{1 - 2s} \sum_{l} |\mu_l|^2\right) (1 - 2s)^{-n} \tag{2.63}$$

and hence T follows a non-central χ^2_{2n} with $\sum_l |\mu_l|^2$ as the non-centrality parameter.

Now, both random variables $|b_1|^2$ and $|b_2|^2$ are unscaled T variables where $n = 1$. We scale the random variable $|b_1|^2$ as follows :

$$|b_1|^2/\left(\xi^2/2\right) = T_1 = \left(\mu_1 + X_1\right)^2$$

with $\mu_1 = \sqrt{2}a/\xi$, $X_1 = \sqrt{2}N_1/\xi$. Similarly we scale the random variable $|b_2|^2$:

$$|b_2|^2/\left(\xi^2/2\right) = T_2 = \left(\mu_2 + X_2\right)^2$$

with $\mu_2 = c_0\mu_1$ and $X_2 = \sqrt{2}N_2/\xi$.

Mean

$$\mathbb{E}(T) = \frac{d}{ds}\Big(E(e^{sT})\Big)\Big|_{s=0} = \left[\left(2(1-2s) + \frac{|\mu|^2}{(1-2s)^2}\right)\exp(\frac{s}{1-2s}|\mu|^2)\right]_{s=0} \tag{2.64}$$

$$= |\mu|^2 + 2 \tag{2.65}$$

$$\Rightarrow \mathbb{E}(|b_1|^2) = a^2 + \xi^2, \tag{2.66}$$

$$\Rightarrow \mathbb{E}(|b_2|^2) = |c_0|^2a^2 + \xi^2 \quad \text{as we found before.} \tag{2.67}$$

From this we deduce that $|\mu_1|^2 = 2(\mathrm{SNR})_1$ and $|\mu_2|^2 = 2|c_0|^2(\mathrm{SNR})_1$.

Variance

$$\frac{d^2}{ds^2}\mathbb{E}(e^{sT}) = e^{\frac{s}{1-2s}|\mu|^2}\Big(\frac{2|\mu|^2}{(1-2s)} - 4 + \frac{4|\mu|^2}{(1-2s)^3} + \frac{|\mu|^4}{(1-2s)^4}\Big) \quad \text{and hence} \tag{2.68}$$

$$\mathrm{Var(T)} = \frac{d^2}{ds^2}\Big(E(e^{sT})\Big)\Big|_{s=0} - (E(T))^2 \tag{2.69}$$

$$= 4|\mu|^2 + 4. \tag{2.70}$$

$$\Rightarrow \mathrm{Var}(|\mathrm{b}_1|^2) = a^2 + 4\xi^2 \tag{2.71}$$

$$\Rightarrow \mathrm{Var}(|\mathrm{b}_2|^2) = a^2|c_0|^2 + 4\xi^2 \tag{2.72}$$

We have thus derived the mean and variance of the general RV $|b|^2$ where

$$b = a + N, \tag{2.73}$$

a is the deterministic signal part and N is a complex Gaussian RV with zero mean and variance ξ^2.. (Reminder: $a = p_0MN_h/2$ for right beam and $a \rightarrow c_0a$ for right beam.)

Hence the above calculation is appropriate for all four random variables $|b_1|^2$, $|b_2|^2$ under the null and alternative hypothesis.

2.5.2 Probability Density Function of a *Non-Central* χ^2 RV

The pdf of a non-central χ^2 distribution can be derived by evaluating the inverse Laplace transform of the moment generating function. We quote the expression from [1] :

If T follows a non-central χ^2_{2n} distribution with non-centrality parameter λ then the density function is

$$f(t|n,\lambda) = \sum_{j=0}^{\infty} \underbrace{e^{-\lambda/2}\frac{(\lambda/2)^j}{j!}}_{A} \underbrace{t^{n+j-1}e^{-t/2}\frac{2^{-(n+j)}}{\Gamma(n+j)}}_{B} \tag{2.74}$$

where A is the probability mass function of the Poisson distribution with parameter $\lambda/2$ and B is the density of a χ^2_{2n+2j} distribution.

We let $n = 1$ in (2.74) and we express it in closed form using I_0, the modified Bessel function of zero order. The pdf of T $\sim \chi^2_2(\lambda)$ is given by

$$f(t|2,\lambda) = \frac{1}{2}e^{-\frac{\lambda+t}{2}}I_0(\sqrt{\lambda t}) \tag{2.75}$$

where

$$I_0(x) = \sum_{k=0}^{\infty}\frac{((1/4)\,x^2)^k}{k!\Gamma(k+1)} = \sum_{k=0}^{\infty}\frac{((1/4)\,x^2)^k}{k!^2} \tag{2.76}$$

The pdf plots under the Null and the Alternative Hypothesis are given in Figures 2.1 and 2.2 respectively.

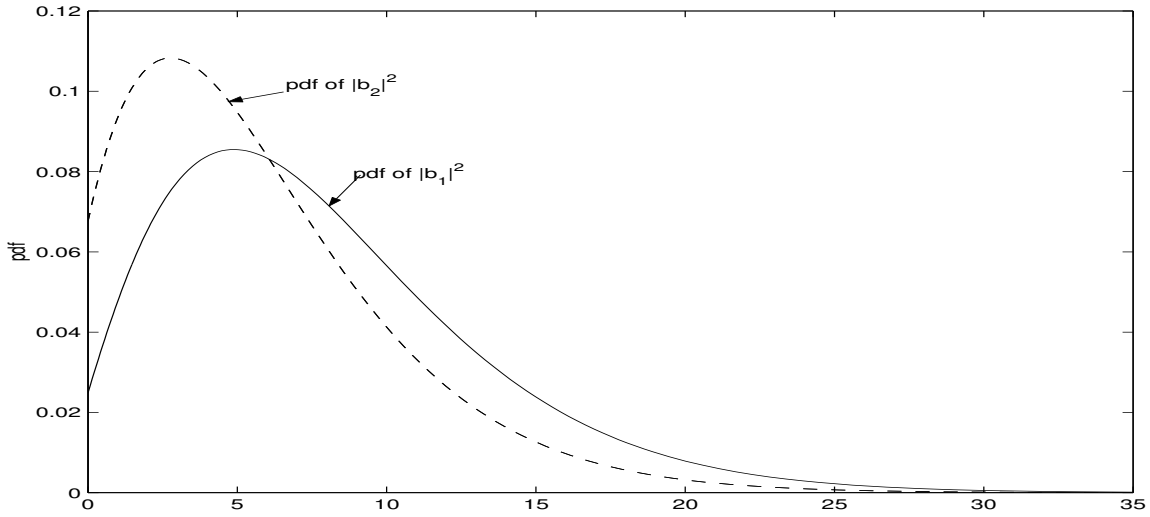

Figure 2.1: Probability density functions if Contact is on the Right (H_0).

Figure 2.2 is exactly the same as Figure 2.1 except that $|b_1|^2$ and $|b_2|^2$ interchange roles. This exhibits the aforementioned symmetry of the statistical test under interchange of the null and alternative hypothesis, to be exploited in the next section.

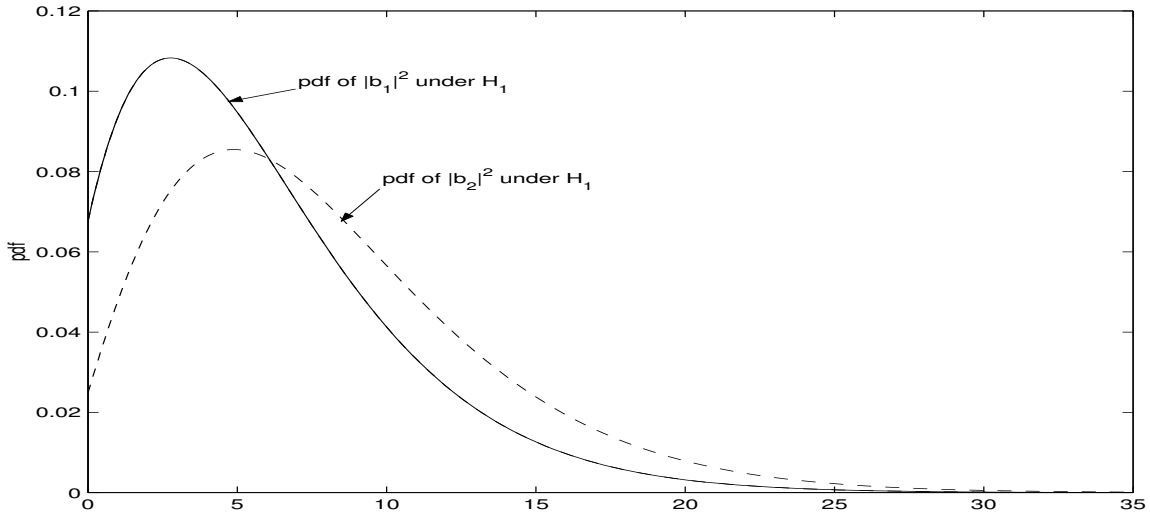

Figure 2.2: Probability density functions if Contact is on the Left (H_1).

2.5.3 The Likelihood Ratio Test

Definition

The Likelihood Ratio L of the data vector $\mathbf{t} = (t_1, t_2)$ with respect to two hypotheses H_0 and H_1 is given by:

$$L_{\mathbf{t}}(H_0, H_1) = \frac{f(t_1, t_2|H_1)}{f(t_1, t_2|H_0)} = \frac{f_1}{f_0} \tag{2.77}$$

The submarine observes $\mathbf{b} = (b_1, b_2)$ (after the DFT).

We define the vector $\mathbf{t} = (t_1, t_2) = \frac{1}{\xi^2/2}(|b_1|^2, |b_2|^2)$, and our hypotheses H_0 and H_1 are respectively that the contact is on the left and right, so that

$$H_0 : T_1 \sim \chi_2^2(\lambda_1) \tag{2.78}$$

$$T_2 \sim \chi_2^2(\lambda_2) \tag{2.79}$$

$$H_1 : T_1 \sim \chi_2^2(\lambda_2) \tag{2.80}$$

$$T_2 \sim \chi_2^2(\lambda_1) \tag{2.81}$$

where

$$\begin{array}{rcl} \lambda_1 & = & |\mu|^2 \\ \lambda_2 & = & |c_0|^2 |\mu|^2 \\ & < & |\mu|^2 \end{array} \tag{2.82}$$

since $|c_0|^2 < 1$.

Under the assumption of uncorrelated noise, N_1 and N_2 are uncorrelated and consequently T_1 and T_2 are uncorrelated. Hence (2.77) reduces to

$$L = \frac{f(t_1|H_1)f(t_2|H_1)}{f(t_1|H_0)f(t_2|H_0)}. \tag{2.83}$$

We thus obtain , using (2.75),

$$L = \frac{I_0(\sqrt{\lambda_2 t_1})I_0(\sqrt{\lambda_1 t_2})}{I_0(\sqrt{\lambda_1 t_1})I_0(\sqrt{\lambda_2 t_2})}. \tag{2.84}$$

According to the Likelihood Ratio Test we are going to reject H_0 if $L = L_1/L_0 > l$ where l is the critical value of the test. Consequently H_1 will be rejected if $L_0/L_1 > \frac{1}{l}$. To have symmetry between H_0 and H_1 we must therefore have $l = 1$. **Hence we reject the hypothesis that the contact is on the right if $L > 1$.**

If we receive a louder signal in the left beam intuitively we would deduce that the contact is on the left and we would reject the null hypothesis. We hence expect that:

$$\text{If } \lambda_2 < \lambda_1 \text{ and } t_2 > t_1 \text{ then } L > 1.$$

To prove this we consider:

$$D = I_0(\sqrt{\lambda_2 t_1})I_0(\sqrt{\lambda_1 t_2}) - I_0(\sqrt{\lambda_1 t_1})I_0(\sqrt{\lambda_2 t_2}) \quad \text{and using(2.76),} \tag{2.85}$$

$$\begin{aligned} D &= \sum_r \sum_s (\frac{2^{-r}}{r!})^2 (\frac{2^{-r}}{r!})^2 (\lambda_2 t_1)^r (\lambda_1 t_2)^s - \sum_r \sum_s (\frac{2^{-r}}{r!})^2 (\frac{2^{-r}}{r!})^2 (\lambda_1 t_1)^r (\lambda_2 t_2)^s \\ &= \sum_{r,s} \{\frac{2^{-2(r+s)}}{r!^2 s!^2}((\lambda_2 t_1)^r (\lambda_1 t_2)^s - (\lambda_1 t_1)^r (\lambda_2 t_2)^s)\}. \end{aligned} \tag{2.86}$$

We now observe that the expression D is invariant under the interchange of r and s and the subscripts 1 and 2. This allows us to write

$$D = \sum_{r=0}^{\infty} \sum_{0 \le s < r} \frac{1}{2^{2(r+s)} r!^2 s!^2}((\lambda_2 t_1)^r (\lambda_1 t_2)^s - (\lambda_1 t_1)^r (\lambda_2 t_2)^s \tag{2.87}$$

$$+ (\lambda_2 t_1)^s (\lambda_1 t_2)^r - (\lambda_1 t_1)^s (\lambda_2 t_2)^r) \tag{2.88}$$

$$= \sum_{r=0}^{\infty} \sum_{0 \le s < r} (\lambda_2^r \lambda_1^s - \lambda_1^r \lambda_2^s)(t_1^r t_2^s - t_1^s t_2^r) C_{r,s} \tag{2.89}$$

$$= \sum_{r=0}^{\infty} \sum_{0 \le s < r} \lambda_1^s \lambda_2^s t_1^s t_2^s (\lambda_2^{(r-s)} - \lambda_1^{(r-s)})(t_1^{(r-s)} - t_2^{(r-s)}) C_{r,s} \tag{2.90}$$

where $C_{r,s}$ denotes the constant positive coefficients in (2.87) Under the assertion

$$\lambda_1 < \lambda_2 \Rightarrow \qquad (\lambda_2^{(r-s)} - \lambda_1^{(r-s)}) < 0$$

$$t_2 > t_1 \Rightarrow \qquad (t^{(r-s)} - t_2^{(r-s)}) < 0$$

and hence $D > 0$ so $L > 1$ as required.

2.5.4 The Probability of Correct Resolution

We have, thus, *proved* that with confidence quantified by $\mathbf{P}(L < 1)$ we decide that the contact is on the right (left) if the response is stronger in the right (left) beam. The size of the critical or rejection region is given by $\mathbf{P}(L > 1)$.

$P(L < 1)$ is the **Probability of Correct Resolution** and it is equal to the power of the test as this is defined above.

We can write this as the integral

$$P(L < 1) = \iint f_0(t_1, t_2) dt_1 dt_2 \tag{2.91}$$

where the region of integration is the region $(t_1 \geq t_2 \geq 0)$. We rewrite $P(L < 1)$ as

$$= \iint f(t_1|H_0) f(t_2, H_0) dt_1 dt_2, \tag{2.92}$$

as T_1 and T_2 are independent RVs. This can be rewritten as

$$P(L < 1) = \int_0^\infty \text{p.d.f.}(t_1)\text{c.d.f.}(t_1) dt_1, \tag{2.93}$$

where c.d.f. stands for cumulative density function and is given by

$$\text{c.d.f.}(t) = \int_0^t \text{p.d.f.}(\tilde{t}) d\tilde{t} = \int_0^t \frac{1}{2} e^{-\frac{\lambda+\tilde{t}}{2}} I_0(\sqrt{\lambda \tilde{t}}) d\tilde{t}. \tag{2.94}$$

In the next chapter we evaluate numerically the Probability of Correct Resolution of the Left-Right Ambiguity for two types of array shape that may appear in practice, as a function of the SNR and $|c_0|^2$; we emphasize that the latter parameter is very important as it quantifies the lateral displacement of the array in comparison with the incident wavelength.

Chapter 3

Applications and Numerical Simulations

In this Chapter we analyse numerically the Probability of Correct Resolution derived in the previous chapter. We examine two cases of practical importance.

3.1 First Case: Sinusoid

For simplicity, we begin by examining the case where the array shape is one cycle of a sine wave[1].

Although the model is quite simple, this shape can be considered adequate for the shape when, as it happens quite often, the submarine is steering with slight oscillatory corrections about its main course.

Since we are interested in determining how the resolution of the left right ambiguity is dependent on the incident wavelength we take the array shape to be

$$y = 2\alpha d \sin(2\pi x/L_0) \tag{3.1}$$

where d is the horizontal spacing between adjacent hydrophones and L_0 is the total length of the array. We see such a shape in Figure 3.1.

Note: Throughout the simulations we have used mostly $d = \lambda/2$ since this is what is used most often in practice ($f = c/\lambda$ is then called the *design frequency*). Hence we can rewrite (3.1) as

$$y = \alpha\lambda \sin(2\pi x/L_0) \tag{3.2}$$

1. $\alpha \geq 0$, dimensionless and constant. $\alpha = 0$ corresponds to a straight array.

2. The lateral displacement of the array increases with α.

[1] In practice the shape of the array is not known and a best estimate is used.

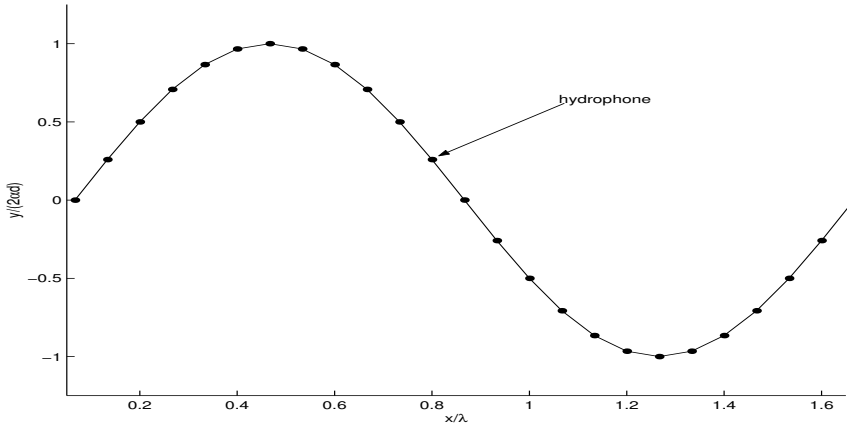

Figure 3.1: Sinusoidal array shape with Number of Hydrophones = 25, $d = \lambda/2$.

So for the jth hydrophone the coordinates are (x_j, y_j) where $y_j = 2\alpha d \sin(2\pi x_j/L_0)$ and $x_j = jd$ where d is the spacing of the hydrophones. We therefore assume that the hydrophones are always equally spaced in the x-direction no matter how deviated is the array from a linear shape. We discuss this assumption as it is quite important for using the programs sensibly.

3.1.1 Validity of the assumption

For the array shape given by (3.2) we let $C = 2\pi/L_0$ and $A = \alpha\lambda$ and let us say that $0 \leq x \leq X$. The arclength along the array is given by

$$ds^2 = dx^2 + dy^2 = dx^2(1 + (AC)^2 \cos^2(Cx)) \tag{3.3}$$

For AC small enough for $(AC)^2$ to be neglected, $ds \approx dx$ and therefore the hydrophones are approximately equally spaced in x and we take $X \approx L_0$, the length of the array.

But for AC not small enough, s is an elliptic integral as a function of x so if $0 \leq s \leq L$ then $0 \leq x \leq X$ with $X < L_0$. This can also be understood intuitively: as the array gets more 'folded' the projections of the hydrophones positions are clearly not kept at a fixed distance from each other.

For example, if we use the values $d = \lambda/2$, $L_0 = (N_h - 1)d$, the dimensionless parameter $\lambda/L_0 = 2/(1 - N_h)$. For $N_h = 25$ we therefore have $AC = \pi\alpha/6$ and hence for values of α somewhat greater than 1 we consider this assumption violated. This is kept in mind while doing the simulations.

Figures 3.2, 3.3 below demonstrate the incoming wave under the hypothesis of a Right or Left contact respectively.

3.2 Second Case: Arc-of-a-Circle shape

For this case we consider the geometry presented in Figure 3.4.

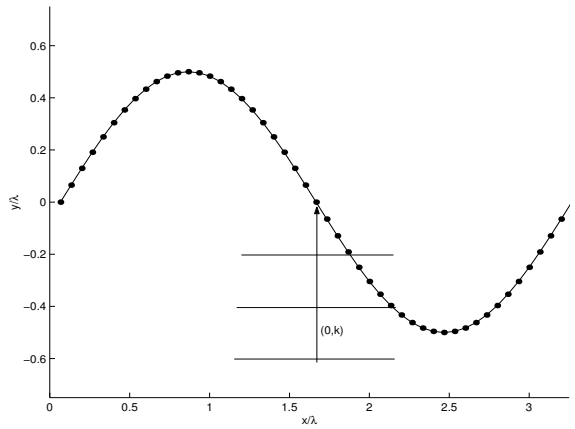

Figure 3.2: Null Hypothesis: Contact on the Right.

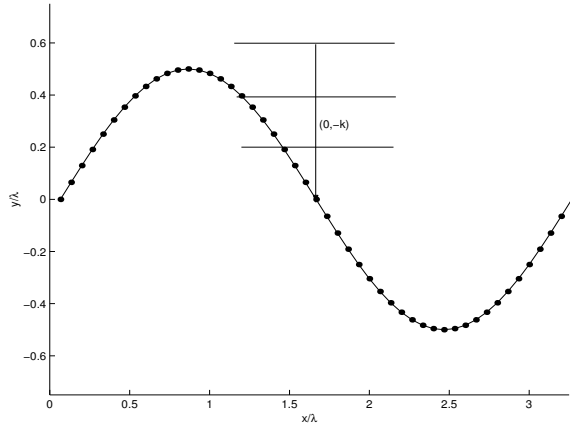

Figure 3.3: Alternative Hypothesis: Contact on the Left.

We consider this to be a model for the array shape when a submarine performs a turn of total angle equal to $2\theta_s$. We observe the array at a time $t < \tau$ where τ is the characteristic timescale of the array dynamics. We consider the length of the array to be *fixed* and hence as θ_s increases the curvature of the arc increases; the radius of the circle obeys the constraint

$$R = \frac{L_0}{2\theta_s}. \tag{3.4}$$

It is also understood intuitively that the larger the change in course direction in the same amount of time, the more bent the array is going to be. In this case the plane polar geometry is allowing us to treat the hydrophones equispaced on the arclength s instead of the horizontal distance x; the inter-hydrophone distance d is given by the arc-length $R\theta_0$ where $\theta_0 = \frac{2\theta_s}{(N_h-1)}$. So no restriction exists on the value of the angle θ_s to make our numerical simulations valid, except from the geometrical contraint $0 \leq \theta_s \leq \frac{\pi}{2}$ (the maximum angle subtended by the arc is π.)

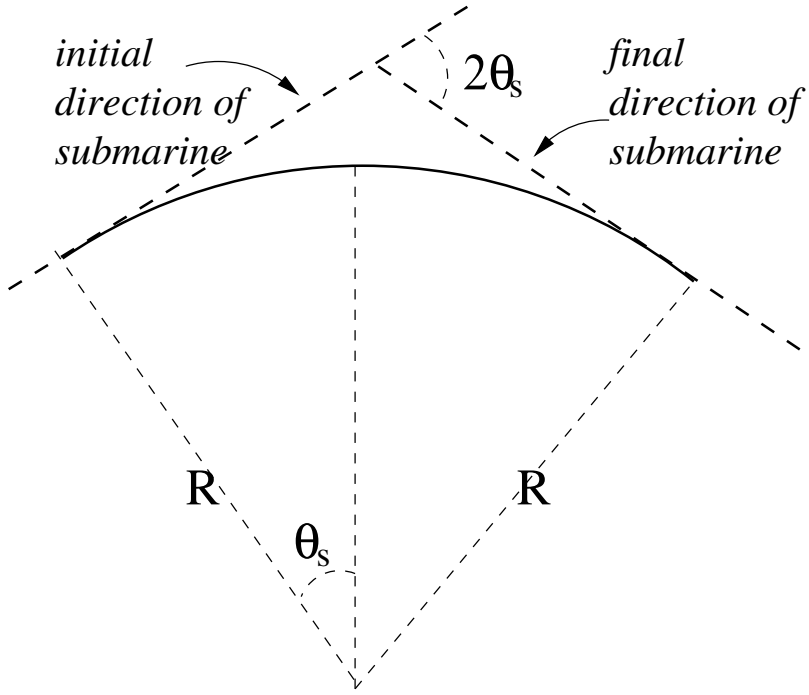

Figure 3.4: The geometry for an array modelled as the arc of a circle.

3.3 Numerical Results

We see that the parameters α and θ_s for the first and second case respectively, defining the size of the lateral displacement of the array, enter the test through the non-centrality parameter $\lambda_2 = |c_0|^2 |\mu|^2$ and specifically through the quantity $|c_0|^2$. As $|c_0|$ is approaching the value 1, that is α is tending to zero, the difference in the response of the left and right beam is diminishing and it is becoming harder and harder to resolve the left-right ambiguity that is, in probability language, we have a smaller and smaller probability of correct resolution. The likelihood ratio L is very near to the critical value of the test $l = 1$ and due to the randomness of the data the transition in or out of the critical region is very easy to happen and hence the decision on whether H_0 or H_1 is true, is being made is more and more equally likely to occur.

Due to the symmetry of the test, we expect that for a *straight* array $\mathbf{P}(\text{Correct Resolution}) = 0.5$. We integrate numerically in MATLAB the Probability of Correct Resolution as a function of the two parameters SNR and $|c_0|^2$. We get for the first case Figure 3.5; for the second case we obtain Figure 3.6.

Notice that the Figure 3.5 is the *same* as 3.6. This comes as no surpise as $\mathbf{P}(L < 1)$ is the *same* function of $|c_0|^2$ and SNR for both Cases. The difference comes in that we are just using different values of $|c_0|^2$ in the *same* range $[0, 1]$ due to the different kind of dependence that $|c_0|^2$ has on the paramter α or θ_s.

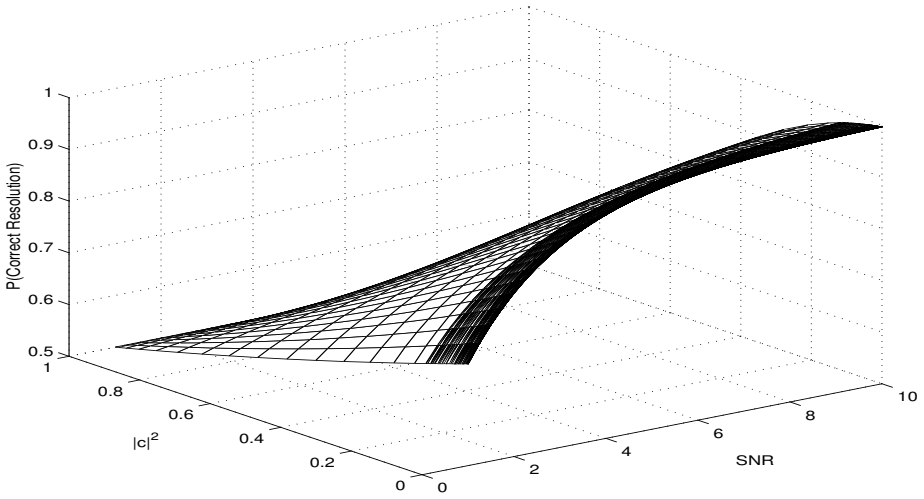

Figure 3.5: The Probability of Correct Resolution as a function of $|c|^2 = |c_0(\alpha)|^2$ and SNR for the Sine Shape.

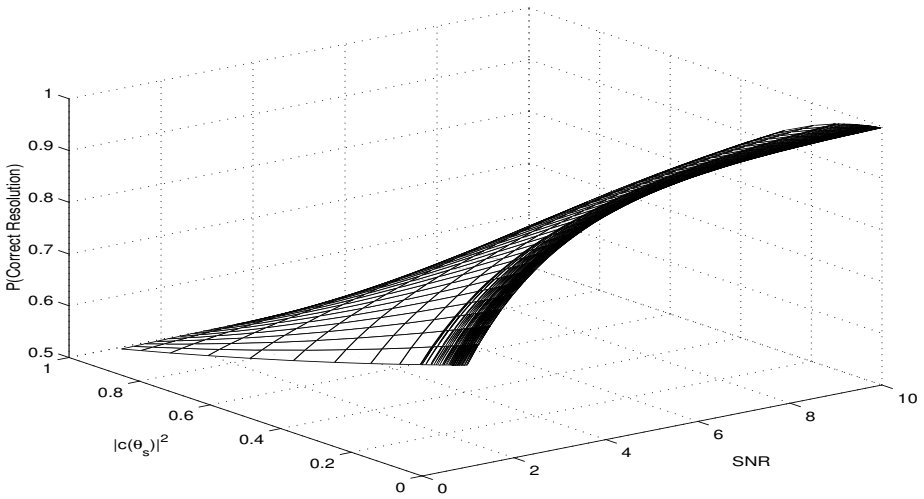

Figure 3.6: The Probability of Correct Resolution as a function of $|c_0(\theta_s)|^2$ and SNR when the array shape is the arc of a circle-θ_s ranges from 0 to $\pi/2$.

We see that we get high probabilities of correct resolution for high values of SNR and small values of the $|c_0|^2$ parameter.

We now investigate the behaviour of $|c_0|^2$ first as a function of α and secondly as a function of θ_s. $|c_0(\alpha)|^2$ exhibits a nice, decaying and oscillatory behaviour as it can be seen in Figure 3.7.

In fact we can find an approximate behaviour for $|c_0|^2$. Since

$$c_0 = \frac{1}{N_h} \sum_{j=1}^{N_h} \exp(4\pi i \alpha \sin(2\pi j / N_h)) \tag{3.5}$$

this can be given approximately by

$$\approx \frac{1}{2\pi}\int_0^{2\pi} \exp(4\pi i\alpha \sin\theta)d\theta \tag{3.6}$$

$$= J_0(4\pi\alpha) \tag{3.7}$$

and hence

$$|c_0(\alpha)|^2 \approx J_0^2(4\pi\alpha). \tag{3.8}$$

which justifies indeed the oscillatory decaying behaviour observed.

3.3.0.1 The Frequency for Best Ambiguity Resolution

We can exploit this result further. $J_0(x) = 0$ for $x = 2.4$, so there is a value $\alpha = \frac{2.4}{4\pi} \approx 0.19$ for which $|c_0(\alpha)| = 0$. This α gives the best probability of correct resolution out of all the range of α (along with the other values of α which correspond to the zeros of J_0 following the first). Hence *we have the best chance to resolve the ambiguity* when $\frac{\text{amplitude}}{\text{wavelength}} = 0.19$, i.e for a given amplitude, there is a certain frequency $f_0 = (0.19c/\text{amplitude})$ at which we get best resolution.

An expression analogous to (3.8) for $|c_0(\theta_s)|^2$ is not available. We observe from Figure 3.8 that the behaviour is still periodic in some extent but after the value $\theta = \pi/3$ the amplitude of the peaks is increasing.

3.3.1 Validity of the Results

We have assumed in doing this analysis that the beams are uncorrelated for all values of α. However, this is not the case for values of α or θ_s near to zero where the array is tending to become straight. This correlation between the beams is quantified by the complex correlation coefficient $\beta = \mathbb{E}(N_1\overline{N}_2)/\mathbb{E}(|N_1|^2)$ (defined in the next chapter). We find there that $|\beta|$ equals 1 when $\alpha = 0$ or $\theta = 0$. When the modulus of the correlation parameter $|\beta| = 1$ the beams are perfectly correlated. However the correlation is decreasing with the increase of α as we see from the plots 4.1, 4.2 and 4.3 in Chapter 4.

Hence the array can have a useful probability of correct resolution if α or θ_s are sufficiently large. The inclusion in the analysis of the non-zero correlation, results to the necessity of tackling a messy integral as we see in the next chapter. However, for values of $\alpha(\theta_s)$ somewhat away from zero our method provides a good estimation of the probability. We see that at α (or θ_s) equal to zero we do obtain $\mathbf{P}(\text{Resolution}) = 0.5$. Our method can be considered even more satisfactory if we bring in mind that none wants to determine where the contact is located when the array is straight, that is the range of very small $\alpha(\theta_s)$ is not of relevance when trying to resolve the LR ambiguity.

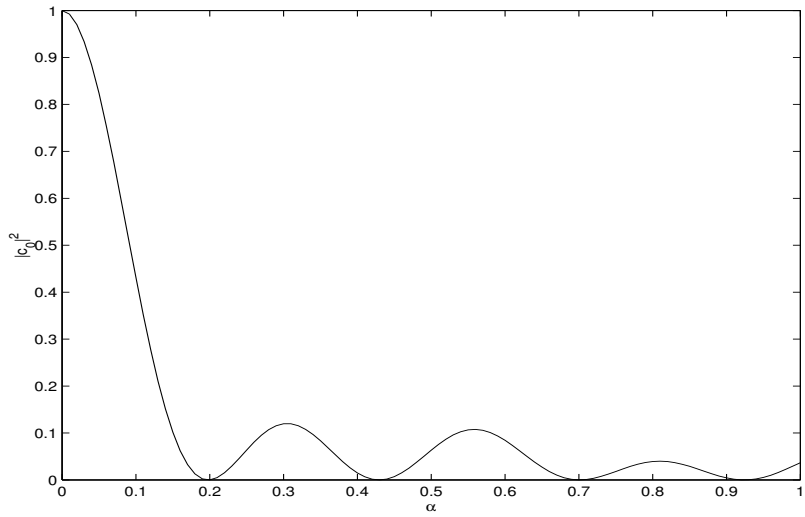

Figure 3.7: $|c_0|^2$ as a function of the lateral displacement parameter α.

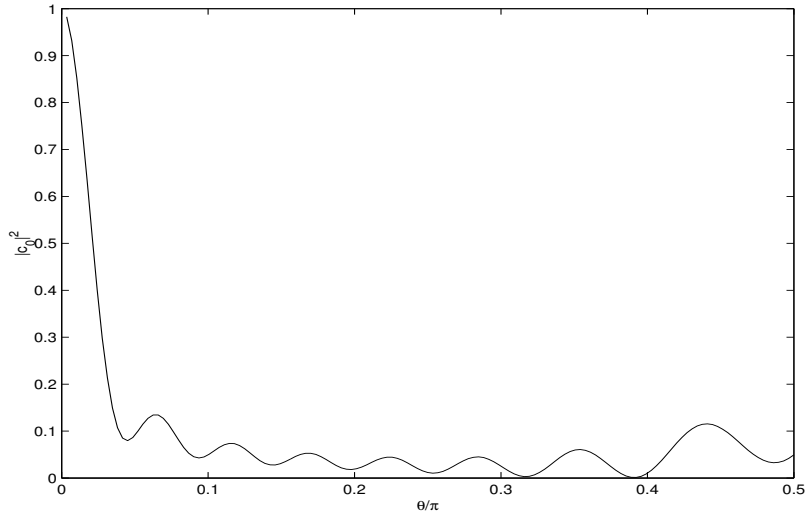

Figure 3.8: $|c_0|^2$ as a function of the angle θ_s.

3.3.2 One-Dimensional Plots

3.3.2.1 Probability of Correct Resolution as $|c_0|^2$ increases (θ_s decreases), SNR *fixed*

We also calculated $|c_0|^2$ as a function of θ_s for fixed SNR and plotted the probability of correct resolution[2]. We see from Figures 3.9 and 3.10 that the probability of correct resolution increases as $|c_0|^2$ decreases. We first fixed SNR at the value 1. We obtained the Figure 3.9. Then we fixed SNR at 5 and we obtained Figure 3.10 and for SNR= 7 we obtained Figure 3.11.

Comparing the figures we see that for larger values of SNR we have larger values of Probability

[2]we can either examine $|c_0\theta_s)|$ or $|c_0\alpha)|$ since Figures 3.5 and 3.6 are the same.

of Correct Resolution. (For example at $|c_0|^2 \sim 0$ in Figure 3.9 (SNR= 1) we have $\mathbf{P} \sim 0.7$, while in Figure 3.10 (SNR= 5) we have $\mathbf{P} \sim 0.9$.)

Note: All above values of SNR are in absolute and not in dB scale.

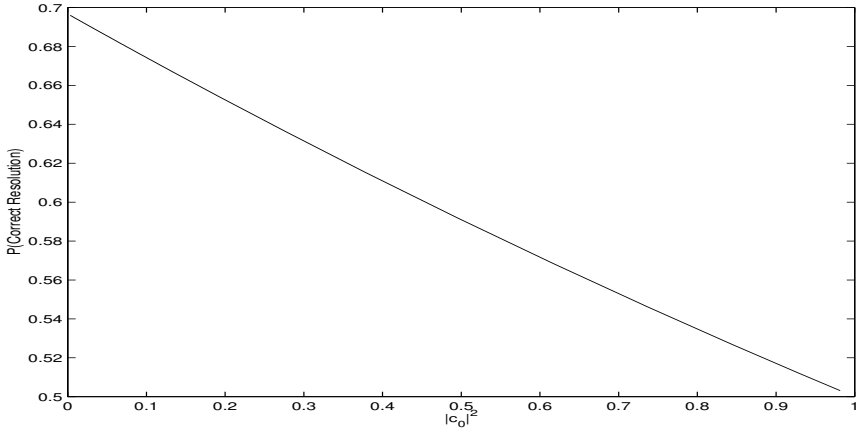

Figure 3.9: Probability of Correct Resolution as $|c_0|^2$ varies from 0 to 1 and fixed SNR= 1.

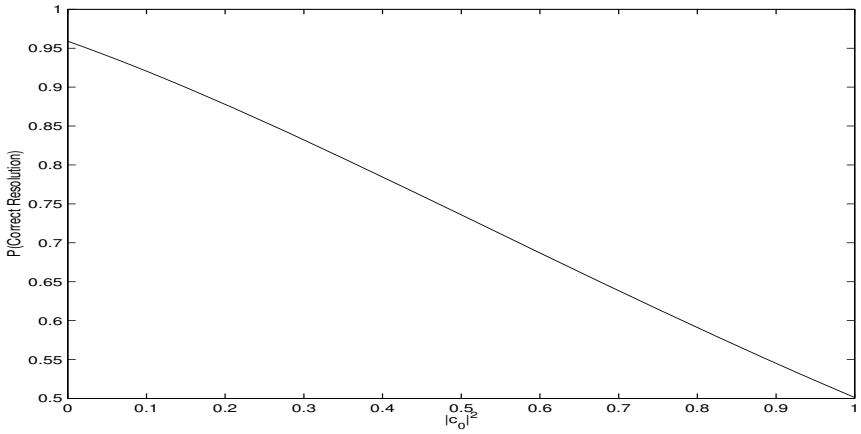

Figure 3.10: Probability of Correct Resolution as $|c_0|^2$ varies from 0 to 1 and fixed SNR= 5.

3.3.2.2 The Probability of Correct Resolution for SNR increasing, $|c_0|^2$ *fixed*

We alternatively fix $|c_0(\theta_s)|^2$ while increasing the SNR. As SNR increases the Probability of Correct Resolution goes to 1 with a trend faster than linear as we can see from Figure 3.12 ($|c_0|^2 = 0.0018$) and Figure 3.13 ($|c_0(\theta_s = 45)|^2 = 0.0429$). We see from Figure 3.12 that for SNR ~ 10 the Probability of Correct Resolution is almost 1 while in Figure 3.13 the Probability does not attain the value 1 within the given range of SNR.

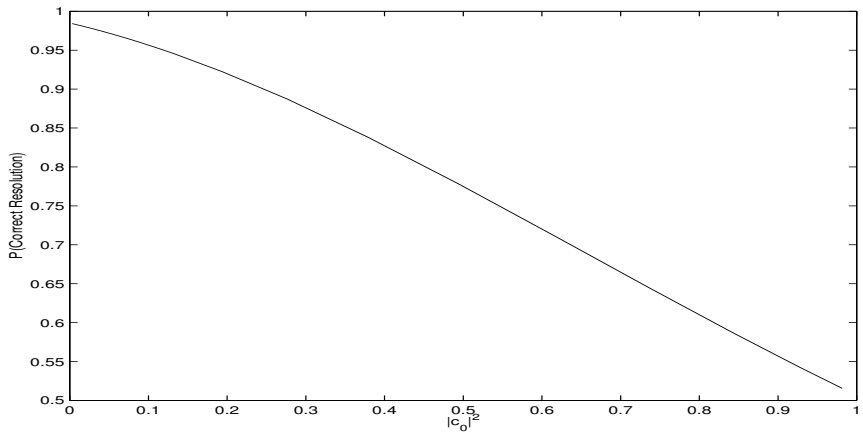

Figure 3.11: Probability of Correct Resolution as $|c_0|^2$ varies from 0 to 1 and SNR= 7.

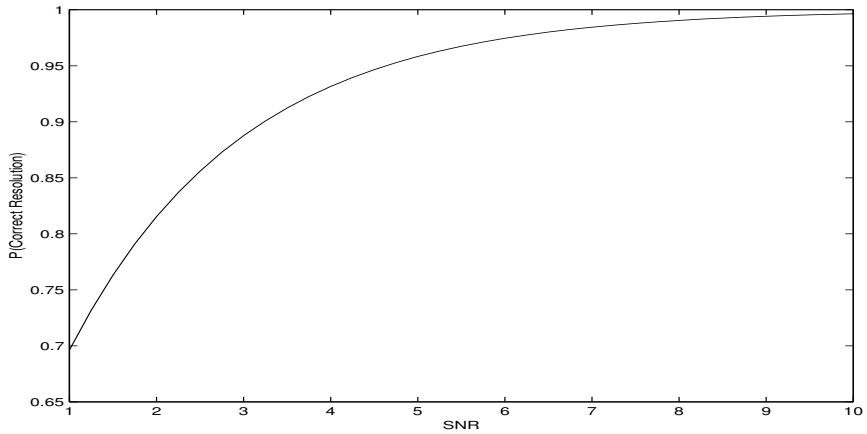

Figure 3.12: Probability of Resolution for $|c_0|^2 = 0.0018$ and SNR varying from 1 to 10 when the array shape is sinusoidal.

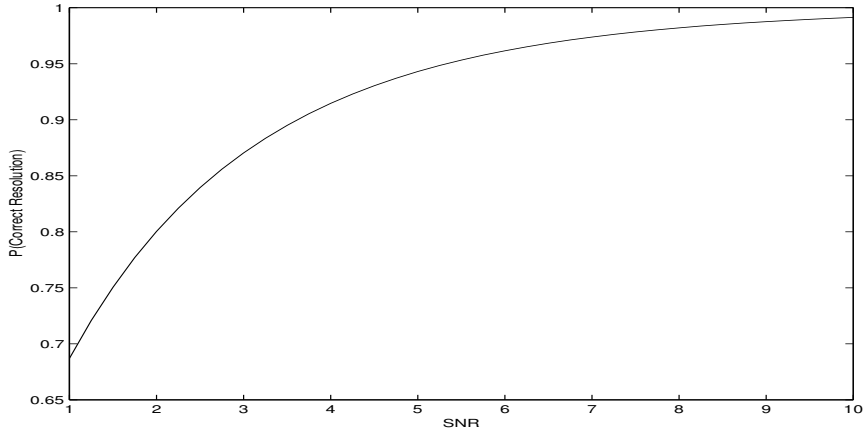

Figure 3.13: Probability of Correct Resolution for $|c_0(\theta_s = 45^0)|^2 = 0.0429$ and SNR varying from 1 to 10-array shape is an arc with subtended angle $2\theta_s = \pi/2$.

Chapter 4

Statistical Analysis- Correlated Noise

4.1 Correlation in the Gaussian Noise

4.1.1 Three-Dimensional Noise Field Correlations

We are aiming to develop a statistical analysis framework analogous to the procedure developed in Chapter 2.

We now drop the assumption that the sea-noise is spatially and temporally uncorrelated and we consider the noise to be modelled as a stationary, homogeneous Gaussian process with mean zero and correlations given by ϕ_n:

$$\mathbb{E}(n(\mathbf{x}_1, t_1)n(\mathbf{x}_2, t_2)) = \phi_n(\mathbf{x}_1 - \mathbf{x}_2, t_1 - t_2) \tag{4.1}$$

where ϕ_n is translationally invariant in the space and time variables. We often represent the correlations ϕ_n with the power spectrum $S_n(\mathbf{k}, \omega)$ and we achieve this using the Fourier transform below:

$$S_n(\mathbf{k}, \omega) = \int_{\mathbb{R}^4} \phi_n(\xi, \tau) e^{i\mathbf{k}.\xi - i\omega\tau} d\xi d\tau \tag{4.2}$$

Writing the Inverse Fourier Transform (IFT):

$$\phi_n(\xi, \tau) = \frac{1}{(2\pi)^4} \int S_n(\mathbf{k}, \omega) e^{-i\mathbf{k}.\xi + i\omega\tau} d\mathbf{k} d\omega \tag{4.3}$$

we can think of the correlation function ϕ_n as a superposition of plane waves $e^{-i\mathbf{k}.\xi+i\omega\tau}$ with weighting coefficients $S_n(\mathbf{k}, \omega)$.

Note that since $n(x, t)$ obeys the wave equation, the power spectral density $S_n(\mathbf{k}, \omega)$ is in fact concentrated on the cone $\omega^2 = c^2|\mathbf{k}|^2$ so $S_n(\mathbf{k}, \omega) = \hat{S}_n(\mathbf{k}, \omega)\delta(\omega^2 - c^2|\mathbf{k}|^2)$. We now use the correlation function to express how any two beams are correlated.

4.1.2 Correlation of Two Beams

We will use the subscripts 1, 2 for the two beams and we denote the time delays by $\Delta_j^{(1)}$, $\Delta_j^{(2)}$. The array samples the continuous noise field $n(\mathbf{x}, t)$ at the positions of the hydrophones, thus creating a finite vector $\mathbf{n} = (n(\mathbf{x}_1, t), ..., n(\mathbf{x}_M, t))^T$.

Hence

$$b_1(t) = \sum_{j=1}^{N_h} n\left(\mathbf{x}_j, t - \Delta_j^{(1)}\right) \tag{4.4}$$

$$b_2(t) = \sum_{j=1}^{N_h} n\left(\mathbf{x}_j, t - \Delta_j^{(2)}\right) \tag{4.5}$$

where we have assumed that the shading weights are $w_j^{(1)} = w_j^{(2)} = 1$ and we have taken only the noise part of the beams. Then we calculate ϕ_{12}, the correlation function between the two beams and using (4.1) we write:

$$\phi_{12}(\tau) = E(b_1(t)b_2(t-\tau)) = \sum_{m=1}^{N_h}\sum_{j=1}^{N_h} \phi_n(\mathbf{x}_j - \mathbf{x}_m, -\Delta_j^{(1)} + \Delta_m^{(2)} + \tau) \tag{4.6}$$

Hence the cross-spectrum between b_1 and b_2 is:

$$S_{12}(\omega) = \int \phi_{12}(\tau)e^{-i\omega\tau}d\tau \text{ and using (4.6) :} \tag{4.7}$$

$$= \sum_{m=1}^{N_h}\sum_{j=1}^{N_h} \int \phi_n(\mathbf{x}_j - \mathbf{x}_m, -\Delta_j^{(1)} + \Delta_m^{(2)} + \tau)e^{-i\omega\tau}d\tau \tag{4.8}$$

$$= \sum_m \sum_j \int \phi(\xi, \tau + \Delta)e^{-i\omega\tau}d\tau \tag{4.9}$$

$$= \sum_m \sum_j e^{i\frac{\omega\Delta}{c}} \int \phi_n(\xi, \tau + \Delta)e^{-i\omega(\tau+\Delta)}d\tau \quad \text{and taking the FT of(4.3)}$$

$$= \sum_j \sum_m e^{i\frac{\omega\Delta}{c}} \iiint S_n(\mathbf{k}, \omega)e^{-i\mathbf{k}.\xi}\frac{d\mathbf{k}}{(2\pi)^3} \tag{4.10}$$

where $\Delta = \Delta_m^{(2)} - \Delta_j^{(1)}$ and $\xi = \mathbf{x}_j - \mathbf{x}_m$.

Hence

$$S_{12}(\omega) = \iiint S_n(\mathbf{k}, \omega) \left(\sum_{j=1}^{N_h} e^{-i\mathbf{k}.\mathbf{x}_j - i\omega\Delta_j^{(1)}/c}\right)\left(\sum_{m=1}^{N_h} e^{i\mathbf{k}.\mathbf{x}_m + i\omega\Delta_m^{(2)}/c}\right)\frac{d\mathbf{k}}{(2\pi)^3} \tag{4.11}$$

and we can write this in the convenient form

$$S_{12}(\omega) = \iiint S_n(\mathbf{k}, \omega)G_1\overline{G_2}\frac{d\mathbf{k}}{(2\pi)^3} \tag{4.12}$$

where G_1 and G_2 are respectively the directivity functions for the beam 1 and beam 2, computed for the incidence vector $\mathbf{u}_1 = -c\mathbf{k}/\omega$.

We observe from (4.12) that although G is introduced as the representation of the action of the beamformer on plane waves, it also characterises the action of the beamformer on the incoming noise. This lies in the fact that the use of the Fourier transform allows us to think of noise as a random superposition of plane waves.

4.1.2.1 The Discrete Fourier Transform

As in Chapters 2 and 3, N_1 and N_2 are complex Gaussian RVs with $\Re N_1 \sim \mathcal{N}(0, \xi^2/2)$, $\Im N_1 \sim \mathcal{N}(0, \xi^2/2)$ and $\Re N_2 \sim \mathcal{N}(0, \xi^2/2)$, $\Im N_1 \sim \mathcal{N}(0, \xi^2/2)$.
The covariance matrix of the complex Gaussian vector $\mathbf{N}$ is given by

$$\mathbb{E}(\mathbf{N}\mathbf{N}^\dagger) = \begin{pmatrix} \mathbb{E}(|N_1|^2) & \mathbb{E}(N_1\overline{N_2}) \\ \mathbb{E}(N_2\overline{N_1}) & \mathbb{E}(|N_1|^2) \end{pmatrix} \tag{4.13}$$

which is no longer diagonal.

- $\beta = \mathbb{E}(N_1\overline{N}_2)/\mathbb{E}(|N_1|^2)$ expresses the strength of the correlation between N_1 and N_2.

Using (4.12) we can write

$$\mathbb{E}(|N_1|^2) = CS_{11}(\omega) = C \iiint S_n(\mathbf{k}, \omega) G_1 \overline{G_1} \frac{d\mathbf{k}}{(2\pi)^3} \tag{4.14}$$

$$\mathbb{E}(|N_2|^2) = CS_{22}(\omega) = C \iiint S_n(\mathbf{k}, \omega) G_2 \overline{G_2} \frac{d\mathbf{k}}{(2\pi)^3} \tag{4.15}$$

$$\mathbb{E}(N_1\overline{N_2}) = CS_{12}(\omega) = C \iiint S_n(\mathbf{k}, \omega) G_1 \overline{G_2} \frac{d\mathbf{k}}{(2\pi)^3} \tag{4.16}$$

$$\mathbb{E}(N_2\overline{N_1}) = CS_{21}(\omega) = C \iiint S_n(\mathbf{k}, \omega) G_2 \overline{G_1} \frac{d\mathbf{k}}{(2\pi)^3} \tag{4.17}$$

ω now is the frequency of sonar contact of interest, and we are assuming this is exactly equal to one of the discrete fourier frequencies (see Chapter 2, section 2.4).
C is a constant produced due to the DFT on the data. For the unwindowed DFT described earlier, $C = M/\Delta t$ where Δt is the sampling interval. A windowed Fourier transform would have the effect of including a numerical factor in C, but the ratios such as β are unaffected.
We can furthermore write

$$\mathbb{E}(|N_1|^2) = \mathbb{E}((\Re N_1)^2) + (\Im N_1)^2) = \xi^2 = \mathbb{E}(|N_2|^2) \tag{4.18}$$

$$\mathbb{E}(N_1\overline{N_2}) = \mathbb{E}(\Re N_1 \Re N_2 + \Im N_1 \Im N_2) - i\mathbb{E}(\Re N_1 \Im N_2 - \Im N_1 \Re N_2) = \xi^2\beta \tag{4.19}$$

$$\mathbb{E}(N_2\overline{N_1}) = \mathbb{E}(\Re N_1 \Re N_2 + \Im N_1 \Im N_2) + i\mathbb{E}(\Re N_1 \Im N_2 - \Im N_1 \Re N_2) = \xi^2\overline{\beta} \tag{4.20}$$

We can, thus, write the covariance matrix of $\mathbf{N}$ also in the following form:

$$V = \begin{pmatrix} \xi^2 & \xi^2\beta \\ \xi^2\overline{\beta} & \xi^2 \end{pmatrix} \tag{4.21}$$

and the p.d.f. of $\mathbf{N}$ is given by

$$f(N_1, N_2) = \frac{1}{\pi^2 \det V} e^{(-\mathbf{N}^\dagger V^{-1}\mathbf{N})} \tag{4.22}$$

$$= \frac{1}{\pi^2 \xi^4 (1 - |\beta|^2)} e^{\left(-\frac{1}{\xi^2(1-|\beta|^2)}(|N_1|^2 + |N_2|^2 - 2\Re(\beta N_1 \overline{N_2})\right)} \tag{4.23}$$

4.1.3 The complex correlation coefficient

We aim to quantify the complex correlation coefficient in the case of broadside contact and a beamformer with only one left and right beam (as it was our simplifying assumption in the previous chapters) as a function of the lateral displacement parameter α for the sine-shape and a function of the parameter θ_s in the case that the array shape is represented by the arc of a circle.

$$\beta = \frac{\mathrm{S}_{12}}{\mathrm{S}_{11}} \tag{4.24}$$

We first consider

$$S_{11}(\omega) = \iiint S_n(\mathbf{k}, \omega) \left(\sum_j e^{-i\mathbf{k}.\mathbf{x}_j - i\omega y_j/c} \right) \left(\sum_m e^{i\mathbf{k}.\mathbf{x}_m i + \omega y_m/c} \right) \frac{d\mathbf{k}}{(2\pi)^3} \tag{4.25}$$

$$S_{11} = \sum_j \sum_m e^{-i\frac{\omega}{c}(y_j - y_m)} \iiint S_n(\mathbf{k}, \omega) e^{-i\mathbf{k}.(\mathbf{x}_j - \mathbf{x}_m)} \frac{d\mathbf{k}}{(2\pi)^3} \tag{4.26}$$

We let $\mathbf{v}_{mj} = \frac{\omega}{c}(\mathbf{x}_m - \mathbf{x}_j)$ and $\mathbf{k} = \frac{\omega}{c}\hat{\mathbf{k}} = \frac{\omega}{c}\zeta$ which is vector over the unit sphere.
We assume that S_n is isotropic and hence we can replace $S_n(\mathbf{k}, \omega)$ with $S_n(|\mathbf{k}|, \omega)$ and write (4.26) as follows:

$$S_{11}(\omega) = \sum_j \sum_m e^{-i\frac{\omega}{c}(y_j - y_m)} \iiint S_n(\mathbf{k}, \omega) e^{i\zeta.\mathbf{v}_{mj}} \frac{d\mathbf{k}}{(2\pi)^3} \tag{4.27}$$

Since ζ lies on the unit sphere we can revert to spherical polar coordinates:

$$\zeta_1 = \sin\phi\cos\theta \tag{4.28}$$

$$\zeta_2 = \sin\phi\sin\theta \tag{4.29}$$

$$\zeta_3 = \cos\phi \tag{4.30}$$

We also let $|\mathbf{k}| = r$ and using (4.28) we rewrite (4.27):

$$S_{11}(\omega) = \sum_j \sum_m e^{i\frac{\omega}{c}(y_j - y_m)} \int_0^{2\pi} d\theta \int_0^{\pi} \int_0^{\frac{\omega}{c}} S(r,\omega) e^{i|\mathbf{v}_{mj}|\cos\phi} \sin\phi dr d\phi \tag{4.31}$$

$$= 2\pi A(\omega) \sum_j \sum_m e^{i\frac{\omega}{c}(y_j - y_m)} \int_0^{\pi} e^{i|\mathbf{v}_{mj}|\cos\phi} \sin\phi d\phi \tag{4.32}$$

$$= 2\pi A(\omega) \sum_j \sum_m e^{i\frac{\omega}{c}(y_j - y_m)} \left[i \frac{e^{i|\mathbf{v}_{mj}|\cos\phi}}{\mathbf{v}_{mj}} \right]_0^{\pi} \tag{4.33}$$

$$= 4\pi A(\omega) \sum_j \sum_m e^{i\frac{\omega}{c}(y_j - y_m)} \text{sinc}\,|\mathbf{v}_{mj}| \tag{4.34}$$

where $\text{sinc}(t) = \sin t/t \;\forall\, t \neq 0$ and $\text{sinc}(0) = 1$. We also have $A(\omega) = \int_0^{\infty} S(r,\omega) dr$.
$A(\omega)$ is proportional to the noise power spectrum at ω, $S_n(\omega)$. We do not determine the constant of proportionality since it subsequently cancels out.
The correlation coefficient contains the information about the array shape through the factor $e^{i\frac{\omega}{c}(y_j - y_m)}$.
We also have

$$S_{22} = S_{11} \quad \text{obvious.} \tag{4.35}$$

$$S_{21} = 4\pi A(\omega) \sum_j \sum_m e^{i\frac{\omega}{c}(y_j + y_m)} \text{sinc}\left(\frac{\omega}{c}\,|\mathbf{x}_m - \mathbf{x}_j|\right) \tag{4.36}$$

$$S_{12} = 4\pi A(\omega) \sum_j \sum_m e^{-i\frac{\omega}{c}(y_j + y_m)} \text{sinc}\left(\frac{\omega}{c}\,|\mathbf{x}_m - \mathbf{x}_j|\right) = \overline{S_{21}} \quad \text{as expected.} \tag{4.37}$$

Hence

$$\beta = \frac{\sum_j \sum_m e^{-i\frac{\omega}{c}(y_j + y_m)} \text{sinc}\left(\frac{\omega}{c}\,|\mathbf{x}_m - \mathbf{x}_j|\right)}{\sum_j \sum_m e^{i\frac{\omega}{c}(y_j - y_m)} \text{sinc}\left(\frac{\omega}{c}\,|\mathbf{x}_m - \mathbf{x}_j|\right)} \tag{4.38}$$

We below plot $|\beta|$ as a function of α (range $[0,1]$, $[0,1.5]$) and θ_s (range $[0, 2\pi]$).

4.1.3.1 Plots of $|\beta|$ as function of α and θ_s

We see that the modulus of the correlation coefficient β decreases as α (or θ_s) increases. After $\alpha \sim 0.2$ the value of $|\beta|$ is less than 0.5. This signifies that when α exceeds 0.2 the Probability of Correct Resolution obtained under the assumption of uncorrelated noise provides a useful approximation in the much more complicated correlated noise case. $|\beta|$ continues decreasing (in an oscillatory manner) when the array shape is sinusoidal but when the array shape is the arc of a circle after $\theta_s \sim \pi/3$ the peaks start increasing after they have shown a decreasing trend. However for the maximum angle $\theta_s = \pi/2$ the amplitude of the nearest peak as we see in 4.3 is still less than 0.5. As we have discussed in Chapter 3 we deduce that in both array shapes of practical importance that are examined, here the uncorrelated noise assumption provides good estimates of the **Resolution Probabilities**.

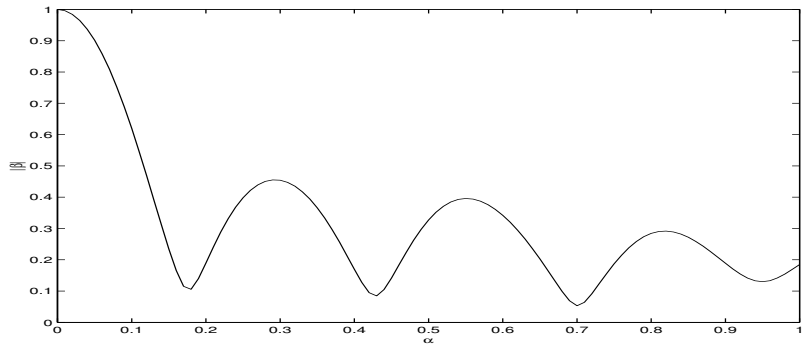

Figure 4.1: $|\beta|$ as a function of α, α from 0 to 1.

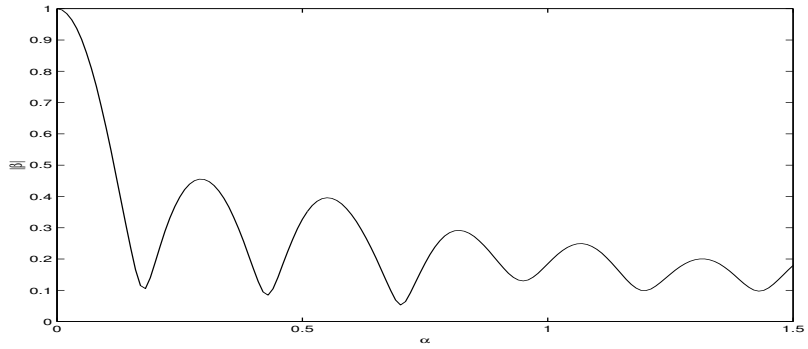

Figure 4.2: $|\beta|$ as a function of α, α from 0 to 1.5.

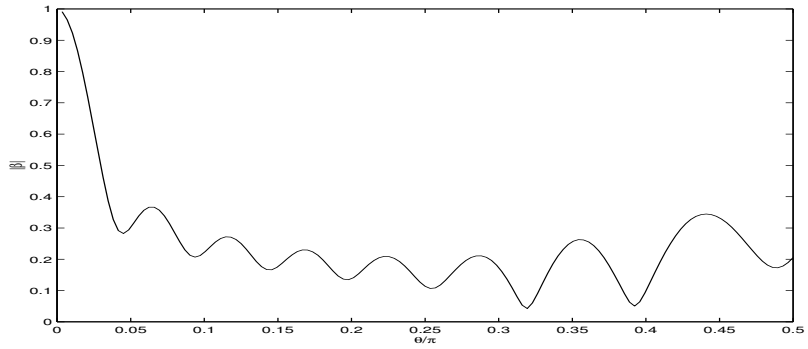

Figure 4.3: $|\beta|$ as a function of θ_s, θ_s from 0 to $\pi/2$.

4.2 Likelihood Ratio Test in the Correlated Noise Case

4.2.1 Hypotheses

Assuming that we have already computed the (discrete) Fourier transform of the incoming signal and noise as in Chapter 2 we again consider, scaling the variables as we did in Chapter 2:

$$H_0 : T_1 \sim \chi_2^2(\lambda_1) \tag{4.39}$$

$$T_2 \sim \chi_2^2(\lambda_2) \tag{4.40}$$

$$H_1 : T_1 \sim \chi_2^2(\lambda_2) \tag{4.41}$$

$$T_2 \sim \chi_2^2(\lambda_1) \tag{4.42}$$

4.2.2 The pdf of the correlated complex random vector Z

Scaling (b_1, b_2) by $\xi/\sqrt{2}$ we obtain the vector

$$\mathbf{z} = (z_1, z_2) = \frac{(b_1, b_2)}{\xi/\sqrt{2}}$$

and $\mathbf{z}$ has a multivariate complex Gaussian distribution given by

$$f(z_1, z_2) = \frac{1}{\pi^2 detV} e^{-(\mathbf{z}-\mathbf{a})^\dagger V^{-1}(\mathbf{z}-\mathbf{a})} \tag{4.43}$$

$$= \frac{1}{\pi^2 \xi^4 (1-|\beta|^2)} \exp\left(-\frac{1}{\xi^2(1-|\beta|^2)}(|z_1-a_1|^2 + |z_2-a_2|^2 - 2\Re(\beta(z_1-a_1)(\overline{z}_2-\overline{a}_2))\right). \tag{4.44}$$

4.2.3 The joint pdf of the correlated RVs $|z_1|^2$, $|z_2|^2$

We aim to derive the joint pdf of $T_1 = |z_1|^2$, $T_2 = |z_2|^2$. Taking the expression

$$|z_1-a_1|^2 + |z_2-a_2|^2 - 2\Re(\beta(z_1-a_1)(\overline{z}_2-\overline{a}_2) \tag{4.45}$$

in the exponent of (4.44) and expanding the moduli, using $z+\overline{z} = 2(\Re z)$, (4.45) becomes:

$$|z_1|^2 + |z_2|^2 + |a_1|^2 + |a_2|^2 - 2\Re(\beta\overline{z}_1 z_2) - 2\Re(\beta\overline{a}_1 a_2) + 2\Re(\beta\overline{z}_1 a_2) + 2\Re(\beta(\overline{a}_1 z_2) - 2\Re(\overline{a}_1 z_1) - 2\Re(\overline{a}_2 z_2) \tag{4.46}$$

Under the null hypothesis $a_1 = a$, $a_2 = c_0 a$. We will revert to the polar representation for z_1, z_2, c_0 and the correlation coefficient β:

$$z_1 = |z_1|e^{i\theta_1} \tag{4.47}$$

$$z_2 = |z_2|e^{i\theta_2} \tag{4.48}$$

$$\beta = |\beta|e^{i\phi_1} \tag{4.49}$$

$$c_0 = |c_0|e^{i\phi_2} \tag{4.50}$$

Note: $\phi_2 = \delta$ in Chapter 2 but here δ employed in a different context.
Hence the expression (4.46)becomes

$$r_1^2 + r_2^2 + a^2(1 + |c_0|^2) - 2|\beta|r_1 r_2 \cos(\theta_2 - \theta_1 + \phi_1) - 2a^2|\beta||c_0| \cos(\phi_1 + \phi_2)$$
$$+2a|\beta||c_0|r_1 \cos(\phi_1 + \phi_2 - \theta_1) + 2a|\beta||c_0|r_2 \cos(\phi_1 + \theta_2) - 2ar_1 \cos\theta_1 - 2a|c_0|r_2 \cos(\theta_2 - \phi_2).$$

To obtain the required pdf of r_1^2 and r_2^2 we have to integrate over θ_1 and θ_2 from 0 to 2π. Choosing to do the integral over θ_1 first, leaving out factors that depend only on r_1^2, r_2^2 and $a^2(1 + |c_0|^2)$,

$$J(r_1, r_2, \theta_2, \phi_1, \phi_2) = \int_0^{2\pi} e^{(-\frac{1}{\xi^2(1-|\beta|^2)}(-2|\beta|r_1 r_2 \cos(\theta_2 - \theta_1 + \phi_1) + 2a|\beta||c_0|r_1 \cos(\phi_1 + \phi_2 - \theta_1) - 2ar_1 \cos\theta_1)} d\theta_1 \tag{4.51}$$

Using

$$\cos(\theta_2 - \theta_1 + \phi_1) = \cos\theta_1 \cos(\theta_2 + \phi_1) + \sin\theta_1 \sin(\theta_2 + \phi_1)$$
$$\cos(\theta_1 - \phi_1 - \phi_2) = \cos\theta_1 \cos(\phi_2 + \phi_1) + \sin\theta_1 \sin(\phi_1 + \phi_2)$$

after grouping together, the parenthesis in the exponent of the integral J becomes:

$$\sin\theta_1 \overbrace{(-2r_1 r_2|\beta| \sin(\theta_2 + \phi_1) + 2a|\beta|r_1|c_0| \sin(\phi_1 + \phi_2))}^{A} \tag{4.52}$$
$$+ \cos\theta_1 \underbrace{(-2ar_1 - 2r_1 r_2|\beta| \cos(\theta_2 + \phi_1) + 2a|\beta||c_0|r_1 \cos(\phi_1 + \phi_2))}_{B} \tag{4.53}$$

We can rewrite as follows:

$$A\cos\theta_1 + B\sin\theta_1 = R\cos(\theta_1 + \delta) \tag{4.54}$$

where $R = \sqrt{A^2 + B^2}$ and $\delta = -\arctan(B/A)$.
We simplify R further:
After expanding A^2 and B^2, using $\sin^2 + \cos^2 = 1$ and $\cos\gamma\cos\delta - \sin\gamma\sin\delta = \cos(\gamma - \delta)$ where $\gamma = \theta_2 + \phi_1$ and $\delta = \phi_1 + \phi_2$ we obtain

$$R^2 = 4a^2 r_1^2(1 + |\beta|^2) + 4r_1^2 r_2^2|\beta|^2 - 8a^2|\beta||c_0|r_1^2 \cos(\phi_1 + \phi_2) \tag{4.55}$$
$$-8ar_1^2 r_2|\beta|(|\beta||c_0| \cos(\theta_2 - \phi_2) - \cos(\theta_2 + \phi_1)) \tag{4.56}$$

where only the last term depends on θ_2.
Using (4.54) and since $\int_0^{2\pi} e^{x\cos\theta} d\theta = 2\pi I_0(x)$ we have

$$J(r_1, r_2, \theta_2, \phi_1, \phi_2) = 2\pi I_0(R(r_1, r_2, \theta_2, \phi_1, \phi_2)). \tag{4.57}$$

The derivation of the joint pdf of $|z_1|^2$ and $|z_2|^2$ still involves the evaluation of the unpleasant integral

$$\int_0^{2\pi} e^{(-\frac{1}{\xi^2(1-|\beta|^2)}(\cos(\theta_2-\theta_1+\phi_1)-2ar_1\cos(\theta_1)+2a|\beta||c_0|r_1\cos(-\theta_1+\phi_1+\phi_2)} \times I_0(R(\theta_2, \phi_1, \phi_2))d\theta_2 \tag{4.58}$$

and this can be achieved only numerically. Once this has been computed, the likelihood ratio L can be formulated as in Chapter 2. Due to the symmetry of the test the critical value will be again $l = 1$. To find the Probability of Correct Resolution we should determine in which *region*, say R_1, of the $(t_1, t_2) = (|z_1|^2, |z_2|^2)$ space, $L < 1$. This turns out to be very tricky in practice. Below the Generalised Likelihood Ratio Test provides however the region R_1 in a very nice manner!
Then

$$P(L < 1) = P(\text{Correct Resolution}) = \iint_{R_1} f_0(t_1, t_2)dt_1dt_2 \tag{4.59}$$

4.3 The Generalised Likelihood Ratio Test

One suggested way to avoid the above integral is to use the *complex* random variables

$$\begin{aligned} b_1 &= a_1 + N_1 \\ b_2 &= a_2 + N_2 \end{aligned}$$

instead of $|b_1|^2$ and $|b_2|^2$. b_1 and b_2 include also the *phases* at the data which is available before the loss effected by the square law detector.

4.3.1 Hypotheses

$$H_0 : b_1 = a + N_1 \tag{4.60}$$
$$b_2 = c_0 a + N_2 \tag{4.61}$$

and

$$H_1 : b_1 = \bar{c_0} a + N_1 \tag{4.62}$$
$$b_2 = a + N_2 \tag{4.63}$$

$$\begin{aligned} \text{Under} \quad H_0 : \quad & a_1 = a \ , a_2 = c_0 a \\ \text{Under} \quad H_1 : \quad & a_1 = \bar{c_0} a \ , a_2 = a \end{aligned}$$

where a is in general complex due to an arbitrary phase added to it depending on how the signal is sampled and Fourier Transformed.

Scaling (b_1, b_2) by $\xi/\sqrt{2}$ we obtain the vector

$$\mathbf{z} = (z_1, z_2) = \frac{(b_1, b_2)}{\xi/\sqrt{2}}$$

and $\mathbf{z}$ has a multivariate complex Gaussian distribution given above by

$$f(z_1, z_2) = \frac{1}{\pi^2 \det V} \exp\big(- (\mathbf{z} - \mathbf{a})^t V^{-1} (\mathbf{z} - \mathbf{a})\big)$$

where $\mathbf{a}$ is the original vector $\mathbf{a} = (a_1, a_2)^t$ scaled by $\xi/\sqrt{2}$.

Now the Generalised Likelihood Ratio is given by

$$L = \frac{\max_{\mathbf{a}} f(z_1, z_2, \mathbf{a}|H_1)}{\max_{\mathbf{a}} f(z_1, z_2, \mathbf{a}|H_0)} = \frac{\max_{\mathbf{a}}(f_1)}{\max_{\mathbf{a}}(f_0)}.$$

We have chosen the Generalised LR as the vector $\mathbf{a}$ is now unknown and we have to obtain the optimum parameter $\hat{a}_0$ that maximises the denominator and $\hat{a}_1$ that maximizes the numerator of L, so that in the end

$$\begin{aligned} &\text{Under} \qquad H_0: \quad a_1 = \hat{a}_0 \ , a_2 = c_0 \hat{a}_0 \\ &\text{Under} \qquad H_1: \quad a_1 = \bar{c_0}\hat{a}_1 \ , a_2 = \hat{a}_1. \end{aligned}$$

$$f_0 = \exp\left\{ \frac{-|z_1 - a|^2 - |z_2 - c_0 a|^2 + 2\Re(\beta(\overline{z_1 - a})(z_2 - c_0 a))}{1 - |\beta|^2} \right\}$$

and we found that this is maximized by

$$\hat{a}_0 = \frac{z_1 + \bar{c_0} z_1 - \bar{\beta}\bar{c_0} z_1 - \bar{\beta} z_2}{1 + |c_0|^2 - 2\Re(\beta c_0)}$$

Similarly f_1 is maximised by

$$\hat{a}_1 = \frac{z_2 + c_0 z_1 - \beta c_0 z_2 - \bar{\beta} z_1}{1 + |c_0|^2 - 2\Re(\beta c_0)}$$

Using

$$z_1 - \hat{a}_0 = \frac{(\beta - \bar{c_0})(z_2 - c_0 z_1)}{1 + |c_0|^2 - 2\Re(\beta c_0)}$$

and

$$z_2 - c_0 \hat{a}_0 = \frac{(z_2 - c_0 z_1)(1 - \bar{\beta}\bar{c_0})}{1 + |c_0|^2 - 2\Re(\beta c_0)}$$

etc., we find that

$$(f_0)_{\max} = k_0 \exp\left(\frac{-|z_2 - c_0 z_1|^2}{1 + |c_0|^2 - 2\Re(\beta c_0)} \right)$$

and

$$(f_1)_{\max} = k_0 \exp\left(\frac{-|z_2 - \bar{c_0} z_1|^2}{1 + |c_0|^2 - 2\Re(\beta c_0)} \right),$$

where k_0 is a constant cancelling out with division.

4.3.2 The Decision Criterion

Hence we accept H_0 if $(f_0)_{\max} > (f_1)_{\max}$ i.e. if

$$|z_2 - c_0 z_1|^2 < |z_1 - \bar{c_0} z_2|^2$$

from which we get

$$|z_2|^2 - 2\Re(z_2 \bar{c_0} \bar{z_1}) + |c_0|^2 |z_1|^2 < |z_1|^2 - 2\Re(z_1 c_0 \bar{z_2}) + |c_0|^2 |z_1|^2,$$

$$\Rightarrow |z_2|^2 (1 - |c_0|^2) < |z_1|^2 (1 - |c_0|^2)$$

and since $|c_0|^2 < 1$ we accept H_0, that is that contact is on the right, when

$$|z_1|^2 > |z_2|^2.$$

This decision criterion is exactly the same as the decision criterion we derived for the uncorrelated noise field in Chapter 2. So although it looked appealing in the beginning to use the additional available phase information on α, the calculation does not improve the test.

4.4 Conclusions

Therefore we draw two important conclusions:

- The test for correlated noise field amounts to rejecting or accepting H_0 using the *same* rule (decision criterion)as in the uncorrelated case! This is saying that we still need to use the joint pdf of $|z_1|^2$ and $|z_2|^2$ in order to draw a conclusion but now we *do* know which (t_1, t_2) region we should integrate over to obtain the Probability of Correct Resolution.
- However, now, as the joint p.d.f. of $|z_1|^2$, $|z_2|^2$ cannot be factored as a product of a function of $|z_1|^2$ only and $|z_2|^2$ only (since z_1 and z_2 are correlated) it seems inevitable to evaluate the tedious integral (4.58) above when calculating the resolution probabilities. The decision criterion gives a very important information; the *region* of integration.

4.5 The moment Generating Function

For completeness we calculate the mgf of $|z_1|^2$ and $|z_2|^2$ in Appendix A. The inverse Laplace transform of the mgf gives, in principle, the joint pdf of the random variables but in practice it is quite tricky to derive the joint pdf in this way.

Chapter 5

Sharpness Function

5.1 The array shape estimation problem and its effect on the beam pattern

Beamforming requires knowledge of the positions of the array hydrophones in order to achieve a reliable output for determining the angle of incidence of a contact signal. Although in systems like Radio Signal Processing the sensor positions are fixed, for a towed, linear array this is not the case. The hydrophone positions change continuously with time. However, the assumption is made that the array has constantly linear shape and the relative hydrophone positions within the array do not change during the beamforming observation time. In practice factors such as fluctuations in the speed and course of the submarine and sea motion, make the array shape nonlinear and consequently significantly *degrade* the beamformer output.

The quality of the beam output is crucial in the resolution of the Left-Right Ambiguity. The data obtained from this output is used in the statistical analysis we developed in the previous chapters and bad beam pattern will make the Probability of Correct Resolution very small.

Various methods have been developed to cope with the problem of the uncertainty in the hydrophone positions. The most common method is to enrich the array with heading and depth sensors. The positions measurements out of these sensors can then be used to construct a polynomial approximation scheme for estimating the array shape.

The use of additional sensors increases significantly the cost and other methods not relying on such external measurement devices has thus been proposed. These much more appealing methods are characterised as *data-driven* methods and estimate the array shape using only information from the received signal.

A great deal of effort is placed in estimating a good array shape and all the following references [3, 4, 8, 9, 14, 16, 21] present possible methods to resolve the problem of array shape estimation which until today cannot be considered resolved.

5.2 Outline of Previous and Our Work

One of the first data-driven methods was proposed by Bucker in 1978[4]. He considered a function which was intended to attain a maximum when the beamformer used the exact array shape to form beams. He called the function the *sharpness function*(SF) after an analogous function introduced in the Optics literature by Muller and Buffington in 1974[15]. The latter SF was maximised only when a telescope produced an image free from atmospheric distortions; this constituted consequently a new technique for 'sharpening' optical images.

Bucker considered this optics idea to be applicable in the Acoustics mindframe but he did not adequately justify his proposition. He performed simulations and deduced that adjusting iteratively the parameters of a simulated array shape until the sharpness function is maximised produces a very good estimate of the true array shape and a sharpened Beam Pattern. In 1990, Ferguson[7] used exactly the same technique, called the Sharpness Method (SM), albeit with a somewhat different beamformer (Adaptive beamformer) and he also reached the conclusion that the method seems reliable in many situations. However, neither Ferguson or Bucker provided a theoretical proof of their results. We proved analytically that their proposition is not valid. We later found that in 1992, Davidson and Cantoni[6] attempted also a proof and they reached the same result. They claimed that the proof cannot be obtained because beamforming and optical imaging bear no similarity. In 1995, Goris, Mareels et al.[12] tried to understand in detail why the sharpness method seems to work in practice. Their results were inconclusive. Goris however pointed out that *noise-free* beamforming and optical imaging are in fact identical procedures if they are formulated in a suitable way. We construct and present a proof of this important statement. We furthermore produce a comparison of the Acoustics and Optics framework. We critisise further the form of the Bucker sharpness function and propose two new functions which we believe to be more suitable to the characteristics of the problem.

We finally connect the SF discussion with the previous chapters that dealt with the Left-Right Ambiguity Resolution and draw a conclusion about the applicability of the SM in the passive sonar context.

5.3 Beamforming formulated differently-revisiting

We have derived the analytical expression of the beam output in the Introduction. This in matrix notation can be written as in Goris [12], p.15,

$$P_b = \mathbf{w}^H R \mathbf{w} \tag{5.1}$$

where $\mathbf{w}$ represents the effect of beamforming and it is given by

$$\mathbf{w} = (\exp(2\pi i \mathbf{u}.\mathbf{x}_1/\lambda), ..., \exp(2\pi i \mathbf{u}.\mathbf{x}_M/\lambda))^T. \tag{5.2}$$

$\mathbf{u} = (\cos\theta_b, \sin\theta_b)$ is a unit vector for the beam in the direction θ_b.
R is the array-covariance matrix or **cross-spectral** matrix, a very important notion in Signal Processing.

$$R = \mathbf{a} R_s \mathbf{a}^\dagger + R_n \tag{5.3}$$

where

$$\mathbf{a} = (\exp(2\pi i \mathbf{u}_s.\mathbf{x}_1/\lambda), ..., \exp(2\pi i \mathbf{u}_s.\mathbf{x}_M/\lambda)^T. \tag{5.4}$$

$\mathbf{u}_s = (\cos\theta_s, \sin\theta_s)$ is a unit vector in the direction of the signal θ_s. R_s is the signal cross-spectral matrix and $R_n = \mathbb{E}(\mathbf{n}\mathbf{n}^\dagger)$ is the noise cross-spectral matrix or noise covariance matrix as given in Chapter 4.

5.4 Sharpness in Optical Imaging

The sharpness method (SM) was developed by Muller and Buffington[15] for correcting atmospherically degraded images. For optical telescopes of aperture[1] D greater than $10 - 30$cm the phase of the incoming signal coming from different paths in the atmosphere is distorted with a variation in the phase dependent on the travelled path. As a result of this phenomenon, since the telescope bases the formation of the image on plane waves, the image will be degraded. They proposed a so-called sharpness function S_1 of which the value of sharpness for an atmospherically degraded image is always less than that of the true image', where S_1 is:

$$S_1 = \int I^2(x, y) dx dy \tag{5.5}$$

where I^2 is the square of the optical power received at the image plane of the telescope. For aperture and image plane see Figure 5.1 [12].

All signals are assumed to reach the telescope from an *isoplanatic patch* of the sky, that is the source of the light is assumed to be of small angular extent. *They proved in their paper that under this assumption S_1 is maximised for an undistorted image.* They implemented the maximisation of this sharpness function using an adjustable mechanism placed before the aperture plane which is able to adjust the phase of the light and cancel the atmospheric disturbances on the same time the measurements are made. S_1 is optimised with respect to the phases introduced by the compensating mechanism.

This mechanism is shown in Figure 5.1 below.

[1]The aperture plane is a circular plane in the telescope receiving the incoming light. We say that the aperture is of size D when the diameter of the circle has value D.

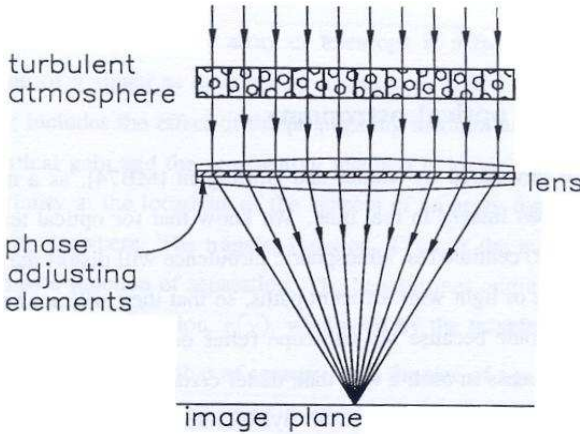

Figure 5.1: Muller and Buffington compensating mechanism for the implementation of the sharpness maximisation in an optical telescope, aperture plane, image plane.

Under the Isoplanatic Patch Assumption a distorted measurement received on the aperture plane $W'(u,v)$, characterised by coordinates (u,v) is

$$W'(u,v) = W(u,v)\Delta(u,v) \tag{5.6}$$

where $W(u,v)$ is the undistorted complex envelope of the *signal* at the telescope aperture. $\Delta(u,v)$ is the effect of atmospheric distortion plus correction from the compensating mechanism.

5.5 Bucker's Work

5.5.1 Definition of the Sharpness Function

Bucker [4] proposed that the following sharpness function S_2 is going to be maximised when the assumed array shape is equal to the true array shape, or in other words when the error in the position of the hydrophones becomes zero.

$$S_2(\hat{y}) = \int_0^{\pi} P_b^2(\phi, \hat{y}) \sin\phi d\phi \tag{5.7}$$

where $\hat{y}$ is the assumed shape of the array. This is in analogy with the SF S_1 proposed by Muller and Buffington.

Notice the existence of the term $\sin\phi$ which comes from the fact that we have switched from Cartesian to polar geometry, where P_b is the Beamformer Output in (5.1).
We now continue working through Bucker's paper.

5.5.2 The assumed array shape

Since the array shape is unknown, he assumes that it is given by the harmonic series expression

$$\hat{y}(t) = \sum_{n=1}^{N} \left(a_n \sin(\frac{n\pi x}{H}) + b_n \cos(\frac{n\pi x}{H}) \right) \tag{5.8}$$

Hence the jth hydrophone is located at the *assumed* position $(\hat{x}_j, \hat{y}_j)$ where

$$\hat{y}_j = \sum_{n=1}^{N_h} \left(a_n \sin(\frac{n\pi \hat{x}_j}{H}) + b_n \cos(\frac{n\pi \hat{x}_j}{H}) \right) \tag{5.9}$$

where $H = L + vT$, L is the length of the array, v is the towing vessel's velocity and T is the time over which the beamformer output is integrated (we used $T = 1s$ in previous calculations).

5.5.3 Validity of the Worm-in-a-hole motion assumption

Bucker does not discuss the validity of this assumption. We think that a brief discussion is quite important.

By assuming that the array shape can be expanded in a harmonic series, it is assumed that the array follows a 'worm-in-a-hole' motion. This means that there is a time-independent function [2]$\hat{y}(x)$ such that the motion of the array obeys $y(s,t) = \hat{y}(x(s,t))\forall$ s,t.

This implies that as the array is moving in the water each point on the array will follow the same path with the first point of the array. More formally this means that the *speed of transverse wave propagation along the array is assumed equal to the speed of the array through water*. But this assumption obviously does not hold at all when the array performs a manoeuvre which drastically changes its orientation in a short amount of time, such as a 90^0 turn for example. The 'worm-in-a-hole' assumption is nevertheless convenient as it provides for use a closed expression for the array shape and and after all it is sufficient for less drastic manoeuvres.

5.5.4 How the coordinates are found as the array is being towed

Bucker says that to find the coordinate of the jth hydrophone at time t, a test point is moved from $(\hat{x}_0, \hat{y}_0)$ along the array in smal linear segment until a distance ξ_j (measured along the array) has been traced and $(\hat{x}_j, \hat{y}_j)$ has been reached.

The underlying procedure is not further explained in the paper but we think it entails the following:
We aim to find $\hat{x}_j$ such that $\xi_j = \int_{\hat{x}_j}^{\hat{x}_0} \sqrt{1 + (\hat{y}'(x))^2} dx$, where ξ_j is known.

Then ξ_j is divided in small linear segments. The ith segment joins the points (x_i, y_i) and (x_{i+1}, y_{i+1}) where $y_i = \hat{y}(x_i)$. We also have $(x_0, y_0) = (\hat{x}_0, \hat{y}_0)$ where $\hat{x}_0 = vt$ and $\hat{y}_0 = \hat{y}(vt)$.

Hence the above integral can be approximated by the discrete sum

[2] $\hat{y}(x)$ can be called the shape of the hole.

$$\xi_j \sim \sum \sqrt{(x_{i+1} - x_i)^2 + (y_{i+1} - y_i)^2} \tag{5.10}$$

We start by using some fixed small $(x_i - x_{i+1}) = \delta x$ and we carry on adding linear segments to the sum until one value of the sum (5.10) is just below ξ_j and the next one is right above ξ_j. Then we use interpolation to decide a final step $< \delta x$ that gives the estimate of the point $(\hat{x}_j, \hat{y}_j)$.

5.5.5 The Bucker Algorithm

Bucker implements his assertion by finding iteratively a best set $(\hat{a}_n^*, \hat{b}_n^*)$ for which $S(\hat{y})$ is maximised or more precisely the discrete approximation to the integral S is maximised. This algorithm is explained in detail by Bucker ([4]) and Goris ([12]) and we present a flowchart of it below as given by Goris.

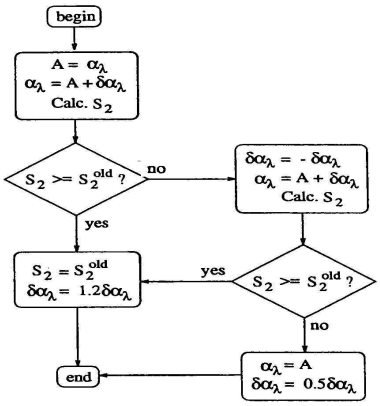

Figure 5.2: Bucker's Algorithm.

He gives two examples, one using real experimental data and the other a simulation. For both cases he obtained very good results; That is he obtains an array shape that is very near to the true array shape and also a beam pattern with high directivity. We include some of his figures below (in the horizontal axis are the steering angles of the beamformer and in the vertical axis is the Beamformer Output in dB). This output is given only from 0 to 180^0 with spacing of 1^0.

Figure 5.3 is before the algorithm has been performed and the array is assumed to be straight. We see that the pattern gives inconclusive information about the incident angle of the signals. Figure 5.4 is after the maximisation of the sharpness function and we can see clearly the three mainlobes corresponding to the sources at angles 30^0, 75^0 and 120^0. We opted to use the Figures from the simulated case because in the experimental situation a very strong source is used (very high SNR) and this is not usually the case with which a submarine has to deal.

However we need to stress one feature of this algorithm: it stops after a *predetermined* number of iterations. It may thus converge to a local and not a global maximum of the sharpness function.

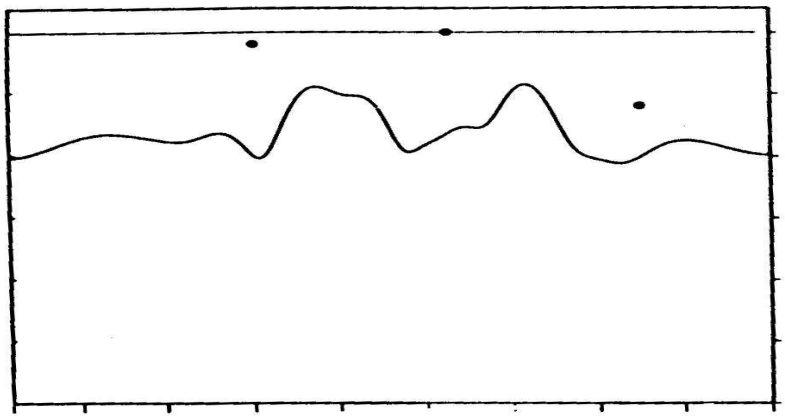

Figure 5.3: The Beam Pattern before Bucker's algorithm has been implemented.

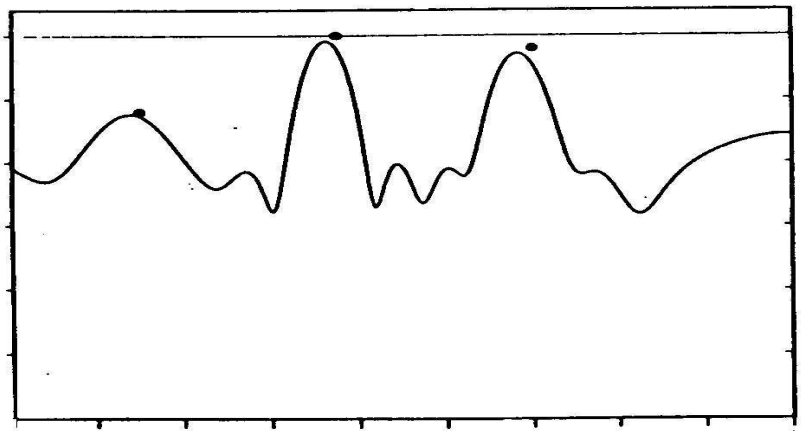

Figure 5.4: The Beam Pattern after Bucker's Sharpness Optimisation Algorithm.

5.6 Ferguson's Work ([7, 8, 9])

He used essentially the same method with Bucker but using a Capon estimator. This is also called an *adaptive beamformer* and it has sharper peaks and lower sidelobes than the conventional beamformer(or *delay-and-sum* beamformer) we have described until now in this work. The beam output for the adaptive beamformer is given by

$$P_b = (\mathbf{w}^H R^{-1} \mathbf{w})^{-1} \tag{5.11}$$

We also present some of his results in Figures 5.5 and 5.6 in which he compares the performance of the beam pattern before and after sharpness function maximisation. He used the same simulated sources as Bucker. The beam pattern of an adaptive beamformer is also compared with that of a conventional beamformer. Although the Figure 5.6 is quite blurred we can see that the beam pattern

is very reliable.

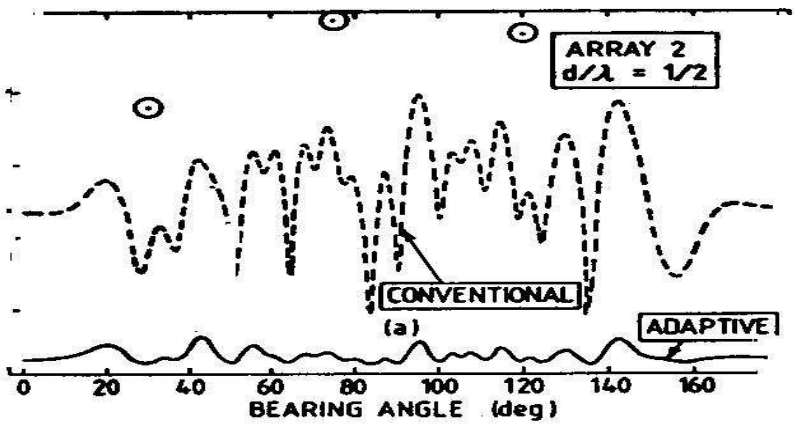

Figure 5.5: The beam pattern is unreliable before the Sharpness maximisation

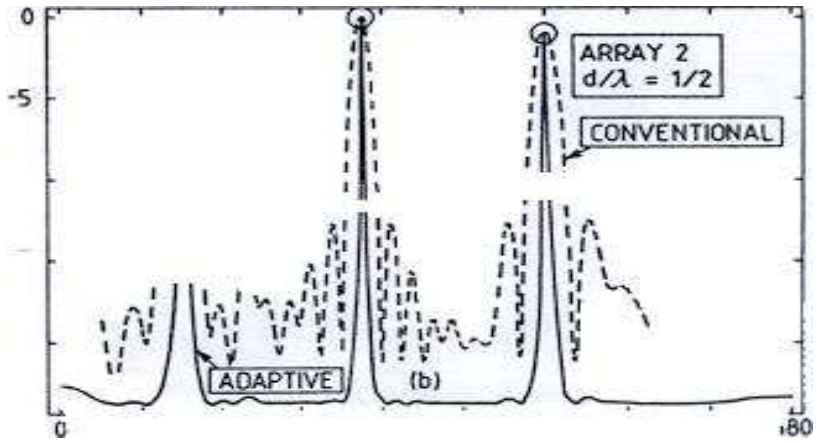

Figure 5.6: The Beam Pattern for a Conventional and an Adaptive Beamformer after Sharpness Maximisation

5.7 Goris Work [12]

Neither Bucker nor Ferguson proved analytically that the sharpness function they used was maximised when the error in the position of the sensors reached zero. Goris has performed his simulations in a much more extended level after an attempt to deal with the Sharpness Function analytically had been made in [6] and had proved to be not fruitful.

He also found out that the Sharpness Method is a good method for array shape estimation assuming that the array is modelled as a superposition of a small number of harmonic terms like Bucker and Ferguson did in their work. However he also found from his simulations that if the array is modelled as a series of straight line segments of fixed length and the sharpness function is

maximised w.r.t. to the angular deviations ϕ_1, ϕ_2 from the horizontal axis then results are not at all satisfactory.

He also investigated what happens when the difference in the angle of incidence of the two signals is varying. He found out that when signals have angles that differ at most by 10^0 then the results are satisfactory. If however, this value is exceeded the results in the beam output degrade significantly and when two sources at $\theta = 90^0$ and $\theta = 150^0$ send signals the true array shape bears no resemblance to the estimated array shape while the beam pattern is completely inconclusive on where the sources are.

This implies that the sharpness method in Acoustics may also need compliance with an analogous Isoplanatic Patch Assumption! It seems that for success of the method the incidence angles of the sources must be very close to each other. Hence Goris results are also inconclusive on whether the Sharpness Method is a Data-Driven Method that can be used safely. As a matter of fact, I. Mareels in a personal communication informed us that until today they still consider the sharpness method to be cumbersome and not reliable at a satisfactory level for obtaining a good array shape.

5.7.1 Analytical Work on the Sharpness Function

Is the Bucker Sharpness Function maximised for the true array shape? We worked out an analytical expression for the sharpness function as such one is not given by Bucker and investigated whether this is maximised when $\hat{y} \Rightarrow y$. The partial derivatives $\partial S/\partial \hat{a}_m$ and $\partial S/\partial \hat{b}_m$ do not vanish when $\hat{y} \Rightarrow y$ so we can deduce that S is not maximised when $\hat{y} \Rightarrow y$. This leads to the unfortunate conclusion that Bucker's method cannot be validated theoretically although it seems to produce good sharpening in the Bucker and Ferguson work.

We know from Goris work that Davidson and Cantoni[6] worked also on the analytical aspects of the sharpness function. Communicating with Davidson we confirmed our results; the sharpness function for the general array shape given by the harmonic series (5.8) is not maximised when the assumed shape is equal to the true array shape.

Davidson and Cantoni claimed that the possible cause to blame for the fact that SF does not produce the correct array shape is that optical imaging and array processing bear no similarity.

This point is wrong as pointed out by Goris; as a matter of fact the noise-free beamforming and formation of optical image are completely analogous processes. We constructed and present here a detailed proof of this.

5.8 Beam Pattern is the same as the optical imaging

We are aiming to prove the complete analogy between the Beam Pattern and the Optical Image. As it is pointed out by Goris

$$\text{Image or Beam Pattern} = IFT(\text{Correlation function of the aperture}),$$

windowed by the *Transfer function*. In more mathematical terms this can also be written as

$$I(\mathbf{x}) = IFT(r(\mathbf{x})T(\mathbf{x})) \tag{5.12}$$

where r is the correlation function (or **V**isibility' function), T is the transfer function, I is the intensity on the image surface and $\mathbf{x}$ is the image vector. The transfer function T is defined as the autocorrelation of the 'pupil' function of the aperture, $p(\mathbf{x})$.

This relationship is already established for the Optical Image ([13], [2]). We need to prove it for the beam pattern.

For this we will define appropriate pupil and transfer functions $p(\mathbf{x})$ and $T(\mathbf{x})$ respectively where $\mathbf{x}$ here denotes *separation* between any two points in the aperture plane. Suppose $s(\mathbf{x}, t)$ is the signal received by the optical/acoustical system. We form

$$z(t) = \int s(\mathbf{x}, t - \Delta(\mathbf{x}))A(\mathbf{x})d\mathbf{x} \tag{5.13}$$

where $z(t)$ will represent the optical image on the beamformer output in the *time-domain*. A is a shading/windowing function which is a continuous analogue of the shading weights w_j. $\Delta(\mathbf{x})$ is a continuous analogue of the time delays. The integral can be 1-dimensional(1D) or 2-dimensional(2D).

Let us take the pupil function for beamforming to be

$$p(\mathbf{x}, t) = A(\mathbf{x})\delta(t + \Delta(\mathbf{x}))$$

an impulse centred at $t = -\Delta(\mathbf{x})$.(we remember that the array samples the noise field at the positions of the hydrophones).

Note The corresponding pupil function for the telescope is given by a 2D indicator function

$$p_0(r, \theta) = \begin{cases} 1, & r \leq R_0 \\ 0, & r > R_0 \end{cases},$$

where R_0 is the radius of the aperture plane.
Hence the transfer function, or the autocorrelation of this pupil function, as it can be proved easily, is an equilateral cone of height R_0 and base of radius R_0.
The Fourier Transform (FT) of $p(\mathbf{x}, t)$ is given by

$$\begin{aligned} \hat{p}(\mathbf{k}, \omega) &= \int p(\mathbf{x}, t)e^{i\mathbf{k}\cdot\mathbf{x} - i\omega t}d\mathbf{x}dt \\ &= \int A(\mathbf{x})\delta(t + \Delta(\mathbf{x}))e^{i\mathbf{k}\cdot\mathbf{x} - i\omega t}d\mathbf{x}dt \\ &= \int A(\mathbf{x})e^{i\mathbf{k}\cdot\mathbf{x} + i\omega\Delta(\mathbf{x})}d\mathbf{x} \\ &= \overline{G(\mathbf{k}, \omega)}, \end{aligned}$$

where G is the directivity function of a beam pattern as it has been defined in the previous chapter. So the autocorrelation of p is

$$\Phi_p(\mathbf{x}, t) = \int p(\mathbf{x}_1, t_1)p(\mathbf{x}_1 - \mathbf{x}, t_1 - t)d\mathbf{x}_1 dt_1.$$

This Φ_p can be called the "transfer function" $T(\mathbf{x})$ of the array aperture.

$$FT\{\Phi_p\} = |G(\mathbf{k}, \omega)|^2 \tag{5.14}$$

by convolution. Then

$$z(t) = \iint s(\mathbf{x}_1, t_1)p(\mathbf{x}_1, t - t_1)dt_1 d\mathbf{x}_1 \tag{5.15}$$

$$= \iint s(\mathbf{x}_1, t_1)A(\mathbf{x}_1)\delta(t - t_1 + \Delta(\mathbf{x}_1))dt_1 d\mathbf{x}_1 \tag{5.16}$$

$$= \int A(ex_1)s(\mathbf{x}_1, t - \Delta(ex_1))d\mathbf{x}_1 \tag{5.17}$$

involves a convolution over time and hence its properties can be expressed in terms of all these quantities.

Now the correlation function of $z(t)$ will be denoted as $\phi_z(\tau)$ where

$$\phi_z(\tau) = \mathbb{E}(z(t)z(t - \tau))$$

and using (5.13) this becomes

$$\begin{aligned} \phi_z(\tau) &= \iint A(\mathbf{x}_1)A(\mathbf{x}_2)\mathbb{E}\big(s(\mathbf{x}_1, t - \Delta(\mathbf{x}_1))s(\mathbf{x}_2, t - \tau - \Delta(\mathbf{x}_2))\big)d\mathbf{x}_1 d\mathbf{x}_2 \\ &= \iint A(\mathbf{x}_1)A(\mathbf{x}_2)\phi_s(\mathbf{x}_1 - \mathbf{x}_2, \tau + \Delta(\mathbf{x}_2) - \Delta(\mathbf{x}_1))d\mathbf{x}_1 d\mathbf{x}_2, \end{aligned} \tag{5.18}$$

We can identify ϕ_s as the autocorrelation of signal and can be thought of as the correlation function $r(\mathbf{x})$.

Let Φ_s be the spectrum of the signal $s(t)$ as given by the inverse fourier transform of ϕ_s (FT of the autocorrelation)

$$\Phi_s(\mathbf{k}, \omega) = \int \phi_s(\mathbf{x}, t)e^{i\mathbf{k}\cdot\mathbf{x} - i\omega t}d\mathbf{x}dt$$

$$\phi_s(\mathbf{x}, t) = \int \Phi_s(\mathbf{k}, \omega)e^{-i\mathbf{k}\cdot\mathbf{x} + i\omega t}\frac{d\mathbf{k}d\omega}{2\pi}. \tag{5.19}$$

Hence using (5.19),(5.18) becomes

$$\phi_z(t) = \iint A(\mathbf{x}_1)A(\mathbf{x}_2)\Phi_s(\mathbf{k}, \omega)e^{-i\mathbf{k}.\mathbf{x}_1}e^{i\mathbf{k}_1.\mathbf{x}_2}e^{i\omega\tau}e^{i\omega\Delta(\mathbf{x}_2)}e^{-i\omega\Delta(\mathbf{x}_1)}$$

and using (5.14)

$$\phi_z(t) = \int \Phi_s(\mathbf{k}, \omega)|G(\mathbf{k}, \omega)|^2 e^{i\omega\tau}\frac{d\mathbf{k}d\omega}{2\pi}.$$

Hence we have proved that the "image" or beam output represented by the power spectrum of z in the *frequency domain* is

$$\Phi_z(\omega) = \int \underbrace{\Phi_s(\mathbf{k},\omega)}_{FT(r(\mathbf{x}))} \mid \underbrace{G(\mathbf{k},\omega)}_{FT(T(\mathbf{x}))} \mid^2 \frac{d\mathbf{k}}{2\pi}$$

so this is indeed the FT of the correlation function of the array aperture *windowed* by the transfer function.

5.9 The proposition of new sharpness functions

The following question arises: Is there another sharpness function which is more appropriate in this case?

We have further noticed that the proposed function S_2 has an important inconsistency in it.

Apparently it is valid for a three-dimensional incoming signal/noise which is incident on a *straight* array. However, the beam power in it is derived on the assumption of a non-straight array.

As we already mentioned, the array is never exactly straight. Hence it is more natural to work in a spherical polar geometry rather than in the planar one. A more appropriate function is then

$$S_3 = \int_{\psi=0}^{2\pi} \int_{\phi=0}^{\pi} \int_0^{\pi} P_b^2(\phi,\psi,\hat{y}) \sin\phi d\phi d\psi \tag{5.20}$$

Another function that is more simple but still more sensible than S_2 is

$$S_4 = \int_{\phi=0}^{\pi} \int_0^{\pi} (P_b^2(\phi,\psi=\pi/2,\hat{y}) + P_b^2(\phi,\psi=-\pi/2,\hat{y})) \sin\phi d\phi \tag{5.21}$$

5.10 Comparison of Acoustics and Optics

	Acoustics	Optics
Aperture	Array Length L	Diameter of the objective lens D
Incoming Signal(input)	Sound($c = 1500$m/s)	Light($c = 3 \times 10^8$m/s)
Output	Beam Pattern(BP)	Optical Image
Measure of image power	sensors	eye
Resolving Power	Direction Accuracy$\sim \lambda/L$	$1.22\lambda/D$
Error	in hydrophone positions	phase distortion in signal
Cause	Hydrodynamics, drag, etc.	Atmospheric Turbulence
Aim	Correct array shape, 'sharpened' BP	Undistorted image

We also stress the differences between the two cases:

1. Difference: The Acoustics case is more complicated because beyond the departure of the array from the true shape (hydrophone position errors) there is also the random effect of

noise. So maximising the sharpness function in Optics eliminates the random phase distortions introduced by the turbulent atmosphere and we get a deterministic image; this is however not plausible in Acoustics; we always remain with the effect of the noise and the features of the beam pattern have to be treated statistically due to the random feature of the noise (noise is modelled as a stationary Gaussian process as we have in the previous chapters).

2. There are many complex effects which account for the dynamical change in the shape of an array that it is being towed. This means that even if random noise did not exist, we would still not be able to obtain the exact array shape due to the fact the array changes its shape continuously with time (dynamics problem) while the telescope problem is static.

3. The speed of light is $c = 3\times10^8$m/s while the speed of sound is $c = 1500$m/s(typical value). The resolving power is of the order of λ/D. Therefore for telescope purposes a typical wavelength is of 6×10^{-7} and with an aperture equal to 20 cm we obtain a resolving power of $\sim 10^{-7}$ radians. However, for an array with $L = 250$m and an incoming wavelength of $\lambda = 15$m the 'resolving power' or direction accuracy is much smaller, $\sim 1/16$ and with the operating frequencies of a sonar$(100 - 250$Hz) we do not have a chance to improve it much further. This leads to the conclusion that Acoustics SM even if analogous in theory to the optics SM, in practice cannot be thought exactly analogous to sharpening a telescope (or camera) image. This happens due to the huge differences in the values of the relevant physical quantities.

4. A telescope is typically used to view light sources directly above the aperture plane of the objective lens. Hence the formation of the image is dependent on the azimuth as well as on the elevation angle (directly above corresponds to an elevation angle of 90^0). We can see that the telescope deals with signal coming from the hemisphere above the aperture plane and the procedure involves spherical geometry. However, in almost all cases the array is assumed to be planar. Hence the array processes signals from the circumference of a circle which is the projection of the telescope hemisphere on the xy-plane and only the azimuth angle is involved.

5.11 Drawbacks and Advantages of the Sharpness Method

1) As it clearly shown in Goris (p.87) in which he compares eight methods of array shape estimation, Sharpness Method is by far the slowest in producing an array shape estimate. This depends on the crudeness of the algorithm.
2) The sharpness method assumes no prior knowledge of signal parameters. This is the fundamental advantage that was the reason for the proposition of the method.

5.12 Critical approach in Connection to the Resolution of the Left-Right Ambiguity

In Bucker 's paper it is argued that the left-right ambiguity has been resolved after the sharpening procedure has been implemented. This conclusion cannot however be reached by looking at the given beam patterns! It is true that the beam pattern seems sharper after the sharpness function has been maximised but the plot is drawn only for steering angles $0 \leq \phi \leq \pi$. We already mentioned that ambiguity exhibits itself in the beam pattern as two mainlobes at the angles ϕ_{contact} and $2\pi - \phi_{\text{contact}}$ so it will be shown only if all steering angles in $[0, 2\pi]$ are shown.

More importantly, when the signal to noise ratio is large we suspect that the method has chances of working. However, submarines operate with low signal to noise ratio situations by definition and consequently we conclude that the method does not provide a good means for towed array shape estimation and beamforming in sonars.

As final remark, talking to I. Mareels, Davidson, and H.P.Bucker we were informed that at the moment they all agree with this result.

Chapter 6

Conclusions

The resolution of the left-right ambiguity problem for a towed array sonar set has been considered theoretically. The successful resolution of the ambiguity always depends on using the fact that the array is not straight, and depends on having some independent estimate of the array shape, such as that provided by heading sensors on the array. We have assumed a simple scenario where a single frequency contact has been detected, and has been located in direction *apart from* the question of resolving the left-right ambiguity. Intuitively, the most natural way of resolving the ambiguity is to form left-pointing and right-pointing beams and decide that the contact is on the left or right according to which beam detects the greater amplitude.

We have analysed this problem mathematically, and find that it is considerably simplified if it is assumed that there is no correlation between the noise in the left and right beams. In that case, the intuitive procedure has been shown to be justified by the likelihood ratio method, and the probability of correct resolution of the ambiguity has been calculated. It depends on the signal to noise ratio of the contact, and it also depends on how much the array deviates from a straight line. If the acoustic wavelength is λ, we considered the case where the array shape is sinusoidal with amplitude $\alpha\lambda$, and calculated the probability of correct resolution of the ambiguity. We showed, for instance, that in order to have 80% probability of correct resolution, the value of α must be at least 1, ie the array deviates from straight by $\pm\lambda$ on each side.

We further considered the problem when *correlation* between the noise in the two beams is taken into account. We have shown that even in this case the intuitive decision procedure is still optimal. We have obtained expressions for the resolution probabilities, but not calculated them. In fact, in cases where there is a useful probability of resolution, the lateral deviation parameter α has to be large, and this in itself causes the correlation between the beams to be small. Hence the results for the *uncorrelated* case should be a good approximation in those parameter ranges where there is good probability of resolution.

We have further considered the "sharpness function" methods. These are intended to provide an improvement in beam patterns by using the received sonar image to further improve estimates

of hydrophone positions. It is important to realise that this method alone cannot resolve ambiguity — the sharpness of a sonar image is unaltered if both the sonar array and the source pattern are reflected in a line. Therefore the previous work on array shape is still fundamental to this method also. However, the sharpness method could conceivably be used to produce further improvements in accuracy etc. We have found a number of important papers and unpublished work relating to the use of the sharpness function in sonar, and have reviewed them. It is clearly an area where there is scope for more detailed analysis, and where application of the method to real sonar data would be an important step. We have shown that the sharpness function

$$S(P_b) = \int_0^{\pi} P_b(\phi)^2 \sin\phi d\phi$$

proposed by Bucker is not well supported theoretically and that a better formulation would be to regard the image P_b as a function over the unit sphere. In this case one would form a sharpness function

$$S(P_b) = \int_{\phi=0}^{\pi} \int_{\psi=0}^{2\pi} P_b(\phi,\psi)^2 \sin\phi \, d\phi \, d\psi.$$

However, the background noise in the sonar context is an aspect whose consequences have not yet been thoroughly studied in this literature. Further work on this would be valuable, but there has not been scope to do this in this dissertation.

Appendix A

The joint mgf of the *correlated* RVs $|z_1|^2$ and $|z_2|^2$

$|z_1|^2 = |a_1 + N_1|^2$ and $|z_2|^2 = |a_2 + N_2|^2$ where N_1 and N_2 are *complex, correlated* Gaussian RVs with covariance matrix V (hermitian).

$$\begin{aligned}
\text{mgf}(|z_1|^2, |z_2|^2) &= M(\underline{s}) = \mathbb{E}(\exp(\sum_{i=1}^{2} s_i |a_i + N_i|^2)) \\
&= \mathbb{E}\exp(\sum_{i=1}^{2}(s_i|a_i|^2 + s_i|N_i|^2 + s_i a_i \bar{N}_i + s_i \bar{a}_i N_i)) \\
&= \exp(\sum_{i=1}^{2} s_i|a_i|^2)\mathbb{E}\left(\exp(\sum_{i=1}^{2} s_i|N_i|^2 + s_i a_i \bar{N}_i + s_i \bar{a}_i N_i)\right) \\
&= \frac{\exp(\sum_{i=1}^{2} s_i|a_i|^2)}{\pi^2|V|} \\
&\quad \times \int_{-\infty}^{\infty} e^{(\sum_{i=1}^{2} s_i|N_i|^2 + s_i a_i \bar{N}_i + s_i \bar{a}_i N_i} e^{-\underline{N}^t V^{-1} \underline{N}} dN_1 dN_2
\end{aligned}$$

where $a_i, s_i \in \mathbb{R},\ 1 \leq i \leq 2$ and for the last equality we have used the pdf of the complex Gaussian vector $\mathbf{N}$. The integral in the last relation can be rewritten using matrix notation:

$$J = \int e^{\underline{N}^t S \underline{N} + \underline{N}^t \underline{v} + \underline{v}^t \underline{N} - \underline{N}^t \underline{V}^{-1} \underline{N}} d\underline{N}$$

where

$$v = S\underline{a} = \begin{pmatrix} s_1 & 0 \\ 0 & s_2 \end{pmatrix} \begin{pmatrix} a_1 \\ a_2 \end{pmatrix}$$

and then

$$J = \int e^{\underline{N}(S - V^{-1})\underline{N}} e^{\underline{N}^t \underline{v} + \underline{v}^t \underline{N}} d\underline{N} \tag{A.1}$$

We write $A = S - V^{-1}$ and diagonalising the Hermitian A with the unitary matrix U:

$$A = U^t \Lambda U \quad \text{and} \quad U\underline{N} = \underline{z}$$

where Λ is a diagonal matrix with *real* eigenvalues $\lambda_1, lambda_2$.

Hence from (A.1) and writing $Uv = \underline{d}$ we obtain

$$\begin{aligned} J &= \int e^{-\underline{z}^t \Lambda \underline{z} + \underline{z}^t \underline{d} + \underline{d}^t \underline{z}} d\underline{z} \\ &= \int e^{\sum_{i=1}^2 \lambda_i |z_i|^2 + \sum_{i=1}^2 \bar{z}_i d_i + \sum_{i=1}^2 \bar{d}_i z_i} d\underline{z} \\ &= \prod_{i=1}^2 \int \underbrace{e^{\lambda_i |z_i|^2 + \bar{z}_i d_i + \bar{d}_i z_i} dz_i}_{J_i} \end{aligned}$$

Hence

$$\begin{aligned} J_i &= \sqrt{\frac{\pi}{\lambda_i}} \exp\left(\frac{(d_i + \bar{d}_i)^2}{4\lambda_i}\right) \cdot \sqrt{\frac{\pi}{\lambda_i}} \exp\left(-\frac{(\bar{d}_i - d_i)^2}{4\lambda_i}\right) \\ &= \frac{\pi}{\lambda_i} \exp\left(\frac{|d_i|^2}{\lambda_i}\right). \end{aligned}$$

Hence

$$\begin{aligned} J &= \frac{\pi^2}{\lambda_1 \lambda_2} \exp\left(\sum_{i=1}^2 \frac{|d_i|^2}{\lambda_i}\right) \\ &= \frac{\pi^2}{\det A} \exp(\underline{v}^t A^{-1} \underline{v}) \end{aligned} \tag{A.2}$$

Hence using (A.2) we get

$$M(\underline{s}) = \frac{\exp(\underline{a}^t S \underline{a})}{\pi^2 \det V} \times \frac{\pi^2}{\det(V^{-1} - S)} \exp(\underline{a}^t S (V^{-1} - S)^{-1} S \underline{a}).$$

We can rewrite

$$M(\underline{s}) = \frac{\exp(\underline{a}^t S \underline{a} + \underline{a}^t S (V^{-1} - S)^{-1} S \underline{a})}{\det V \det(V^{-1} - S)}.$$

Reformating the exponent using a series of simple manipulations we obtain

$$M(\underline{s}) = \frac{\exp(\underline{a}^t (S^{-1} - V)^{-1} \underline{a})}{\det V \det(V^{-1} - S)}. \tag{A.3}$$

References

[1] M. Abramowitz and I.A. Stegun. *Handbook of Mathematical Functions.* Wiley, New York, 1971.

[2] Max Born. *Principles of Optics.* Pergamon Press, Oxford, 6th edition (cor.) edition, 1993.

[3] M. Bouvet. Beamforming of a distorted line array in the presence of uncertainties in the sensor positions. *J. Acoust. Soc. Am.*, 81:1833–1840, 1987.

[4] H.P. Bucker. Beamforming a towed line array of unknown shape. *J. Acoust. Soc. Am.*, 63:1452–1454, 1978.

[5] W. B. Davenport and W. L. Root. *An introduction to the theory of random signals and noise.* Lincoln Laboratory publications, 1958.

[6] T.N. Davidson and A. Cantoni. Towed Array Shape Estimation using the Sharpness Concept. Technical report, University of Western Australia, 1992.

[7] B.G. Ferguson. Sharpness applied to the adaptive beamforming of acoustic data from atowed array of unknown shape. *J. Acoust. Soc. Am.*, 88:2695–2701, 1990.

[8] B.G. Ferguson. Comparison of Sharpness and Eigenvector methods for towed array shapeestimates. *J. Acoust. Soc. Am.*, 91:1565–1570, 1991.

[9] B.G. Ferguson. Remedying the effects of array shape distortion on the spatial filtering of acoustic data from a line array of hydrophones. *IEEE Journal of Oceanic Engineering*, 18:565–571, 1993.

[10] T.M. Ferguson. Probability and Mathematical Statistics, a series of Monographs and Textbooks. In *Mathematical Statistics-A Decision Theoretic Approach.* Academic Press, New York ; London, 1967.

[11] N.R. Goodman. Statistical Analysis based on a certain multivariate complex Gaussian distribution. (An introduction). *Annals of Mathematical Statistics*, 34:152–177, 1963.

[12] M.J. Goris. *Shape Estimation in broadband acoustic beamforming.* PhD thesis, Australian National University, 1995.

[13] J.P. Hamaker, J.D. O'Sullivan, and J.E. Noordam. Image Sharpness, Fourier Optics, and redundant-spacing interferometry. *J. Opt. Soc. Am. Letters*, 67:8, 1122–1123, 1977.

[14] B.E. Howard. Calculation of the Shape of a towed underwater acoustic array. *IEEE Journal of Oceanic Engineering*, 17:193–203, 1992.

[15] R.A. Muller and A. Buffington. Real-time correction of atmospherically degraded telescope images through image sharpening. *J. Opt. Soc. Am.*, 64:1200–1210, 1974.

[16] B.G. Quinn. The estimation of the shape of an array using a hidden Markov model. *IEEE Journal of Oceanic Engineering*, 18:557–563, 1993.

[17] A.C. Rice. *Mathematical Statistics and Data Analysis*. Duxbury Press, Belmont, California, 1995.

[18] Urick. *Principles of Underwater Sound*. McGraw-Hill, New York, 1975.

[19] H.L. Van Trees. *Detection, Estimation and Modulation Theory-Part I*. John Wiley and Sons, New York, 1968.

[20] H.L. Van Trees. *Detection, Estimation and Modulation Theory-Part III*. John Wiley and Sons, New York, 1971.

[21] D.E. Wahl. Towed array shape estimation using Frequency-wavenumber data. *IEEE Journal of Oceanic Engineering*, 18:583–590, 1993.

[22] A.D. Waite. *Sonar for Practising Engineers*. Thomson Marconi Sonar Limited, New York, 1998.